ResearchGate

See discussions, stats, and author profiles for this publication at: https://www.researchgate.net/publication/262230840

Secondary Organic Aerosol Composition from C 12 Alkanes

ARTICLE *in* THE JOURNAL OF PHYSICAL CHEMISTRY A · MAY 2014

Impact Factor: 2.69 · DOI: 10.1021/jp501779w · Source: PubMed

CITATIONS
5

READS
31

8 AUTHORS, INCLUDING:

Katherine A. Schilling
California Institute of Technology
16 PUBLICATIONS **289** CITATIONS

SEE PROFILE

Christine L Loza
California Institute of Technology
27 PUBLICATIONS **670** CITATIONS

SEE PROFILE

Xuan Zhang
Aerodyne Research Inc.
19 PUBLICATIONS **205** CITATIONS

SEE PROFILE

Available from: Xuan Zhang
Retrieved on: 25 January 2016

THE JOURNAL OF PHYSICAL CHEMISTRY A

Article

pubs.acs.org/JPCA

Secondary Organic Aerosol Composition from C_{12} Alkanes

Katherine A. Schilling Fahnestock,[†] Lindsay D. Yee,[‡,§] Christine L. Loza,[†,∥] Matthew M. Coggon,[†] Rebecca Schwantes,[‡] Xuan Zhang,[‡] Nathan F. Dalleska,[‡] and John H. Seinfeld*[,†,‡]

[†]Division of Chemistry and Chemical Engineering, California Institute of Technology, Pasadena, California 91125, United States

[‡]Division of Engineering and Applied Science, California Institute of Technology, Pasadena, California 91125, United States

Supporting Information

ABSTRACT: The effects of structure, NO_x conditions, relative humidity, and aerosol acidity on the chemical composition of secondary organic aerosol (SOA) are reported for the photooxidation of three C_{12} alkanes: *n*-dodecane, cyclododecane, and hexylcyclohexane. Acidity was modified through seed particle composition: NaCl, $(NH_4)_2SO_4$, and $(NH_4)_2SO_4 + H_2SO_4$. Off-line analysis of SOA was carried out by solvent extraction and gas chromatography−mass spectrometry (GC/MS) and direct analysis in real-time mass spectrometry. We report here 750 individual masses of SOA products identified from these three alkane systems and 324 isomers resolved by GC/MS analysis. The chemical compositions for each alkane system provide compelling evidence of particle-phase chemistry, including reactions leading to oligomer formation. Major oligomeric species for alkane SOA are peroxyhemiacetals, hemiacetals, esters, and aldol condensation products. Furans, dihydrofurans, hydroxycarbonyls, and their corresponding imine analogues are important participants in these oligomer-producing reactions. Imines are formed in the particle phase from the reaction of the ammonium sulfate seed aerosol with carbonyl-bearing compounds present in all the SOA systems. Under high-NO conditions, organonitrate products can lead to an increase of aerosol volume concentration by up to a factor of 5 over that in low-NO conditions. Structure was found to play a key role in determining the degree of functionalization and fragmentation of the parent alkane, influencing the mean molecular weight of the SOA produced and the mean atomic O:C ratio.

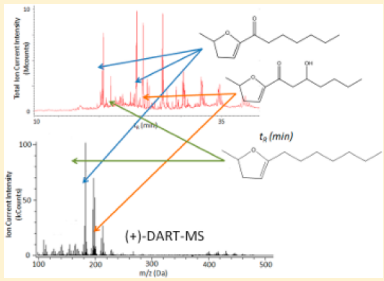

INTRODUCTION

Secondary organic aerosol (SOA) formation generally proceeds by the multigeneration gas-phase oxidation of volatile organic compounds (VOCs) followed by condensation of the oxidized products into the aerosol phase.[1] It has been well-established that once in the particle phase, oxidation products may undergo additional chemistry, including oligomerization reactions.[2−8] A dominant issue in a particular VOC system is the extent of particle-phase chemistry in its SOA formation. Oligomerization has in some cases been observed to occur within seconds of the onset of particle formation and, in addition, can be sensitive to the presence of acidic species.[3,4,8] Low-volatility, high-molecular weight oligomers can influence the particle's phase state.[9−11] The molecular characterization of the particle phase holds the key to identifying particle-phase chemistry in SOA formation.

Cyclic, branched, and linear alkanes constitute a large fraction of gasoline and diesel fuel.[12] Moreover, alkane combustion and photooxidation products are known to be important contributors to urban and transportation-related SOA.[12−15] Alkane SOA composition has been reported in a number of studies (Table 1).[15−30]

These studies encompass both flow tube and environmental chamber photooxidation of C_6 to C_{27} alkanes with cyclic, linear, and branched structures under high- and low-NO conditions. Observed photooxidation products are hydroxycarbonyls, alcohols, aldehydes, and carboxylic acids, as well as more complex species such as furans, lactones, and peroxyhemiacetals. Combined experimental and modeling studies point to the importance of oligomer formation under low-NO oxidation of *n*-dodecane.[32,35,36] Targeted studies showed that peroxyhemiacetals can be important contributors to alkane SOA formation under low-NO conditions when both aldehydes and hydroperoxides are present in the gas phase.[25,36]

Particle-phase chemistry of carbonyl groups is known to lead to relatively complex structures; for example, 1,4-substituted hydroxycarbonyl compounds form cyclic hemiacetals that can dehydrate to form dihydrofurans.[37] 1,4-hydroxycarbonyls are found in both the gas and particle phases and when additionally substituted may participate in further particle-phase chemistry. Aldehydes are known to undergo imine formation in the presence of amines, but none of the studies to date has investigated nitrogen incorporation in the organic aerosol phase, other than the nitration of secondary alkane sites under high-NO conditions.[38−40] Imines are an important constituent of "brown carbon", a broad category of chromophoric organic material that impacts the optical properties of atmospheric aerosol.[41] Gas- and particle-phase chemical analyses employed in these previous studies provide a foundation for interpreting

Special Issue: Mario Molina Festschrift

Received: February 19, 2014
Revised: May 8, 2014
Published: May 9, 2014

ACS Publications © 2014 American Chemical Society

Table 1. Prior Alkane SOA Composition Studies

alkane system	experimental conditions	technique employed	types of products identified	reference
cholestane ($C_{27}H_{48}$)	flow tube reactor, OH-initiated heterogeneous oxidation	2D-GC/ToF-MS (EI or VUV)	ketones, aldehydes, alcohols, hydroxyketones	Zhang et al.[15]
C_5-C_8 *n*-alkanes	chamber-based OH oxidation with NO	SPME/GC-FID	hydroxyketones	Reisen et al.[16]
hydroxy-aldehydes	chamber-based OH oxidation	Tenax and SPME/GC-FID	alcohols, aldehydes	Baker et al.[17]
squalane ($C_{30}H_{62}$), octacosane	flow tube reactor, OH-initiated heterogeneous oxidation	2D-GC/ToF-MS	carbonyls, alcohols, lactones, hydroxyketones, carboxylic acids	Ruehl et al.[21]
$C_{15,16}$ *n*-alkanes, $C_{12,15}$ cyclic alkanes, 2,6,10-trimethyldodecane	chamber-based high-NO_x OH oxidation	thermal desorption particle beam MS (TDPB-MS)	dihydrofurans, alkyl nitrates, hydroxyketones	Lim et al.[22]
C_{6-17} linear alkanes, $C_{6-8,10,12,15}$ cyclic alkanes, C_{6-11} branched alkanes	chamber-based high-NO_x OH oxidation	TDPB-MS	dihydrofurans, alkyl nitrates, hydroxyketones	Lim et al.[23]
C_{8-15} alkanes	chamber-based high-NO_x OH oxidation	TDPB-MS	hydroxy-nitrates, dinitrates, substituted tetrahydrofurans	Lim et al.[24]
$C_{6,7,8,10}$ cyclic monoalkenes	chamber-based ozonolysis, reaction of alcohols with stabilized Criegee intermediates	TDPB-MS	alkoxy hydroperoxy aldehydes, peroxyhemi-acetals (PHA)	Ziemann[25]
n-dodecane	chamber-based OH oxidation	chemical ionization MS (CIMS), aerosol MS (AMS)	hydroxycarbonyls, hydroperoxycarbonyls, hydro-peroxides, peracids, PHA	Yee et al.[28] Craven et al.[31]
n-dodecane, 2-methylundecane, hexylcyclohexane, cyclododecane	chamber-based OH oxidation	CIMS, AMS	hydroxycarbonyls, hydroperoxides, hydroperoxy carbonyls, acids, PHA	Yee et al.[32]
$C_{10,15,17}$ *n*-alkanes tricyclo[5.2.1.0]-decane, diesel fuel, crude oil	PAM flow reactor with OH oxidation	AMS	no speciation; O:C ratios 0.13−1.33	Lambe et al.[33]
cyclo $C_{8,10,15}$, pentyl- and decylcyclohexane, pristane ($C_{19}H_{40}$), 7-methyltridecane, 2-methylundecane, *n*-dodecane	environmental chamber, OH oxidation under high-NO_x conditions	AMS	no speciation; O:C ratios from 0.1 to 0.5	Tkacik et al.[34]

dependence of alkane SOA composition resulting from changes in reaction conditions or parent compound structure.

We report characterization of the chemical composition of SOA generated in the low- and high-NO oxidation of three C_{12} alkanes: *n*-dodecane, hexylcyclohexane, and cyclododecane. We also report the first application of direct analysis in real-time mass spectrometry (DART-MS) to off-line filter samples to determine SOA composition; this method allows us to identify intact compounds, including species prone to reactive loss and decomposition. Off-line analysis of SOA allows the application of a variety of softer ionization conditions, preserving functionalities not detected in aerosol mass spectrometry (AMS). Reactive DART-MS using ion trap mass spectrometry allowed the confirmation of hydroperoxide and peroxide functional groups. Gas chromatography − mass spectrometry enabled the resolution of isomeric species and provided structural information. We address the evidence for particle-phase chemistry in each of these three alkane systems through detailed analysis of the particle-phase composition. By the combination of these two mass spectrometry approaches, we are able to report close to 100% identification and quantification of the particle phase for each of the three alkane systems. In all, 750 individual mass spectral features are identified, and 324 isomers are resolved. We begin with a description of the experimental techniques applied, followed by a discussion of the compositions for each of the three alkane systems. Plausible reaction mechanisms associated with the key identified species are presented.

■ EXPERIMENTAL SECTION

SOA formation from oxidation of three C_{12} alkanes (Table 2) was studied in the dual 24 m^3 Teflon reactors in the Caltech Environmental Chamber, which is described elsewhere.[28,29,42]

Hydroxyl radicals were generated via photolysis of hydrogen peroxide using black lights with a peak wavelength of 350 nm. H_2O_2 (280 μL of 50% wt. solution, Sigma-Aldrich) was measured with a glass syringe (Hamilton) and injected into a glass trap, which was then immersed in a water bath (35−38 °C) while 5 L min^{-1} of filtered air flowed through the trap into the chamber. H_2O_2 was volatilized over the course of 90 min under these conditions, producing an initial mixing ratio of approximately 4 ppm. An aqueous solution of ammonium sulfate was prepared from solid ammonium sulfate (>99.9%, Sigma-Aldrich) and water (18 MΩ, Milli-Q). Ammonium sulfate seed aerosol was produced by atomizing a 0.015 M aqueous solution into the chamber, providing a 15−20 μm^3 cm^{-3} volume concentration. Atomization of aqueous solutions of 0.015 M NaCl (Sigma-Aldrich, >99%) and $(NH_4)_2SO_4$ mixed with H_2SO_4 (Sigma-Aldrich, 18 M) produced seed aerosol at similar volume concentrations in selected experiments (Table 3).

Teflon filters (Pall Life Sciences, 47 mm, 1.0 μm pore size), on which SOA was collected, were cleaned prior to aerosol collection by sonication in a 50/50 (v/v) mixture of heptane (Aldrich, Chromasolv, >99%) and acetone (EMD, Omnisolv, 99.5%). The filters were dried in glass Petri dishes under a gentle stream of UHP nitrogen on an aluminum block heated to 35 °C. Once dry, the filters were stored in glass scintillation vials with Teflon-lined caps prior to use. Aerosol was collected on filters in parallel at flow rates of 17 ± 1 and 23 ± 1 L min^{-1} for 2 h.

Analysis of SOA by DART-MS. Filter samples were analyzed using two different DART-MS systems: a JEOL

Table 2. C_{12} Compounds Studied

Parent Compound	Structure	P_{vap}[a] at 25 °C (atm)	k_{OH} x 10^{12} [b] (cm^3 $molec^{-1}$ s^{-1})
n-Dodecane	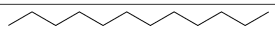	2.59 x 10^{-4}	13.9
Hexylcyclohexane	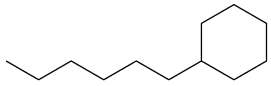	4.1 x 10^{-4}	13.1
Cyclododecane	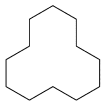	1.64 x 10^{-4}	14.7

[a]Using EVAPORATION.[43] [b]Calculated using relative rate from *n*-dodecane k_{OH} in the University of Leeds' Master Chemical Mechanism (MCM).[44]

AccuToF DART-MS and the custom-built Caltech mini-DART source on a Thermo LTQ ion trap mass spectrometer. The combination of both instruments provided both accurate mass measurements and MS/MS data to confirm adduct identities.

The JEOL DART-MS was operated with the discharge electrode set to +5 kV and subsequent electrodes set to +150 and +250 V. Helium flow was set at 1 L min^{-1}, and the source was heated to 200 °C. Mass calibration was performed for accurate mass measurement in both positive and negative modes by the analysis of a standard solution of PEG-600 in methanol. Solids were analyzed by placing a small piece in the DART stream with stainless steel forceps. Solutions were analyzed by dipping a glass capillary in the solution and placing the capillary tip in the DART stream. A 1 cm wide swath was cut from the center of each filter using clean stainless steel surgical scissors. The filter membrane piece was wrapped around the tip of clean stainless steel forceps and placed in the path of the DART stream until the ion current began to decline after reaching a maximum, indicating that most of the available organic material had been removed during analysis.

The mini-DART source that we employed offers flexibility in the ionizer configuration as well as the ability to conduct MS^2 experiments with the ion trap mass spectrometer. The needle electrode was operated at a DC potential of 3−5 kV with a current between 0.2 and 1.0 mA. The filter electrode was maintained at a potential of +110−250 V, based on prior studies with other DART systems.[45−48] The helium flow was 1.0 L min^{-1}, and the source temperature was 200 °C. The outlet of the mini-DART was oriented for direct flow into the mass spectrometer inlet at a distance of 1−3 cm; the sample, prepared identically to those analyzed on the JEOL instrument, was manually introduced into this space. Additional standard analyses using the mini-DART to assess analyte response across a broad range of vapor pressures using polypropylene glycol, cocaine, and heroin are included in the Supporting Information.

Homologous compound standards were analyzed under conditions identical to those of chamber SOA samples to identify ionization artifacts and to validate interpretation of DART mass spectra. A precleaned Teflon filter was spiked with 100 μL of a 4 ppm standard containing *n*-dodecane (Sigma-Aldrich, 99+%), 2-dodecanol (Aldrich, 99%), 2-dodecanone (Aldrich, ≥97%), 1,12-dodecanediol (Aldrich, 99%), and dodecanoic acid (Sigma, ≥99%) in heptane/acetone (50/50, v/v). The filter was analyzed in the same manner as the chamber samples. For calibration of liquid samples, a clean glass capillary was dipped into the 4 ppm standard mixture and analyzed. Benzoyl peroxide, lauroyl peroxide, and *tert*-butylperoxy benzoate were analyzed individually by dipping a clean glass capillary into an aliquot of each neat compound then passing it through the DART stream. For confirmation of the presence of primary amines (in this case, ammonia), a syringe with a 2 mM solution of 18-crown-6 in methanol was primed to load a droplet onto the needle tip. The 18-crown-6 droplet was cointroduced into the DART stream with the peroxide liquid sample. Ammonium ion adducts disappear with introduction of 18-crown-6 and are replaced by proton adducts ($[M + H]^+$). Further discussion of this procedure as well as example mass spectra appear in the Supporting Information.

Targeted quantitative analysis by DART-MS requires the presence of an internal standard, typically one that is isotopically labeled so as to have the same vapor pressure and proton affinity as the analyte.[49] Choosing an internal standard is more difficult in the case of a complex mixture of unknown compounds with a range of vapor pressures. The ideal internal standard for SOA analysis would be an organic compound with a vapor pressure and proton affinity similar to that of the projected components, be present solely in the particle phase at a mixing ratio near that of the photochemical products, but be nonparticipatory in particle-phase reactions. Such an ideal standard has not been identified, so an alternative internal standard was chosen. Dibutyl phthalate is present in the Teflon filters used to collect the particles; it can be considered to be in excess with respect to individual SOA components. It is also assumed that its ion current intensity is proportional to the DART stream spot size and other transient ionization conditions.

Vapor pressures and proton affinities must be similar for the internal standard and average predicted analyte. Semivolatile compounds have vapor pressures between 10^{-5} and 10^{-11} atm, and compounds composing aerosol have vapor pressures below about 10^{-11} atm.[50] Dibutyl phthalate has a vapor pressure of 5.93×10^{-9} atm at 298 K.[51] This vapor pressure is within the range of expected analyte vapor pressures but biased toward the semivolatile range. Dibutyl phthalate forms a proton adduct ($[M + H]^+$, m/z 279.1591) in positive-mode DART ionization.[52,53] Proton affinity (PA) is defined by the reaction of $M + H^+ \rightarrow MH^+$, where $\Delta H_{rxn} = -PA$, and PA is reported in kilojoules per mole.[54] The estimated PA for the average predicted alkane SOA compound is on the order of ∼839 kJ mol, based on the PA values for homologous compounds (4-methylcyclohexanone (844.9 kJ mol^{-1}), ethyl methyl carbonate (842.7 kJ mol^{-1}), *n*-propyl acetate (836.6 kJ mol^{-1}), *n*-dipropyl ether (837.9 kJ mol^{-1}), 4-heptanone (845.0 kJ mol^{-1}), tetrahydro-2-methylfuran (840.8 kJ mol^{-1}), and 2,5-dihydrofur-

Table 3. Summary of Experimental Conditions[a]

parent VOC	$[VOC]_0$ (ppb)	oxidant precursor	$[NO]_0$ (ppb)	$[NO_2]_0$ (ppb)	$[O_3]_0$ (ppb)	T (°C)	RH (%)	seed	seed volume ($\mu m^3 cm^{-3}$)	total organic volume ($\mu m^3 cm^{-3}$)
n-dodecane	321	H_2O_2	ND	ND	ND	24.11	3.3	$(NH_4)_2SO_4$	20	167
n-dodecane	359	H_2O_2	ND	ND	ND	23.9	54.1	$(NH_4)_2SO_4$	35	56
n-dodecane	245	H_2O_2 + NO	97.5	ND	ND	23.2	5.6	$(NH_4)_2SO_4$	15	376
n-dodecane	342	H_2O_2	7.9	ND	ND	23.9	2.8	$MgSO_4 + H_2SO_4$	14	74
n-dodecane	366	H_2O_2	ND	ND	ND	23.6	59.7	NaCl	32	80
n-dodecane	339	H_2O_2	ND	ND	ND	24.0	2.4	NaCl	15	138
hexylcyclohexane	457	H_2O_2	ND	ND	ND	24.1	3.3	$(NH_4)_2SO_4$	21	265
hexylcyclohexane	332	H_2O_2 + NO	120.1	ND	ND	23.1	4.5	$(NH_4)_2SO_4$	16	748
cyclododecane	330	H_2O_2	ND	ND	ND	24.0	5.1	$(NH_4)_2SO_4$	19	144
cyclododecane	293	H_2O_2 + NO	102.1	ND	ND	22.5	4.0	$(NH_4)_2SO_4$	14	767

[a]Aerosol samples collected by filtration during final 2 h of photooxidation. ND = not detected (limit of detection is 5 ppb). In the fourth *n*-dodecane experiment, 7.9 ppb of NO was not added deliberately and did not affect the experimental outcome significantly. Total organic volume is wall-loss corrected.

an (823.4 kJ mol^{-1})).[55] The proton affinity of dibutyl phthalate can be estimated from its homologue, dimethyl *p*-phthalate (843.2 kJ mol^{-1}).[55] The difference between the estimated PA for the internal standard, dibutyl phthalate, and the average predicted alkane SOA compound is ∼0.5%. There is good agreement between the internal standard and predicted analyte PA, and the assumption that the ratio of the internal standard and analyte PA is ∼1 holds for this predicted system.

A relationship between analyte concentration and ion current must be established next. For DART-MS, the ion current intensity I of any species is proportional to the concentration C, vapor pressure P_{vap}, and proton affinity A: $I = AP_{vap}C$. This equation is written for both the analyte (A) and the internal standard (IS) and then ratioed, allowing for the cancellation of the proton affinity term. Analyte vapor pressures were estimated by using the EVAPORATION model; imine functional groups are not included in the EVAPORATION model, but their vapor pressures were estimated from their carbonyl analogues because of the first-order similarity in bond polarity between carbon and oxygen or nitrogen.[43] When rewritten to solve for the ratio of the concentration of analyte to the concentration of the internal standard, the equation becomes

$$\frac{C_A}{C_{IS}} = \frac{P_{vap,IS}}{P_{vap,A}} \frac{I_A}{I_{IS}}$$

The dominance of one or a few compound classes makes it preferable to use the log of the ratio of concentrations of analyte to internal standard for each compound and summed for each compound class. The relative concentrations for each compound class allows for comparison between functional group abundances. To calculate the mean molecular weight for each chamber SOA sample, these relative concentrations were summed to obtain the total. Using the total, a percentage contribution for each compound was obtained, and that was used as the weighting factor for each compound in calculating the mean molecular weight. A further discussion of this calculation procedure appears in the Supporting Information.

From the formulas obtained by DART-ToF-MS analysis, H:C and O:C ratios were calculated and plotted on a van Krevelen diagram[56] to depict the trends in functionalization and fragmentation for each chamber SOA sample. Typically, a van Krevelen diagram is generated from high-resolution aerosol mass spectrometery data, where each data point on the diagram corresponds to the bulk SOA chemical composition at a specific time point. Here, each data point represents a specific compound detected by DART-MS. The van Krevelen diagram has been developed as an interpretation of HR-MS data to visualize the functionalization of complex organic mixtures.[30,33,56−62] The slope of a line drawn between or through points in a van Krevelen diagram represents the extent of addition or loss of C, H, or O atoms, which when interpreted with the source HR-MS data obtained by soft ionization, translates to the net differences in functionality between the detected compounds.[33,60] From this type of analysis, the distribution of products from a chamber SOA sample can be visualized and interpreted along the lines representing hydration, peroxide formation or alcohol addition, ketone or aldehyde formation, carboxylic acid formation, or nitrate addition. The line with slope = −1, for example, can represent both a carboxylic acid group addition or the addition of both a carbonyl group and a hydroxyl group to the same compound;

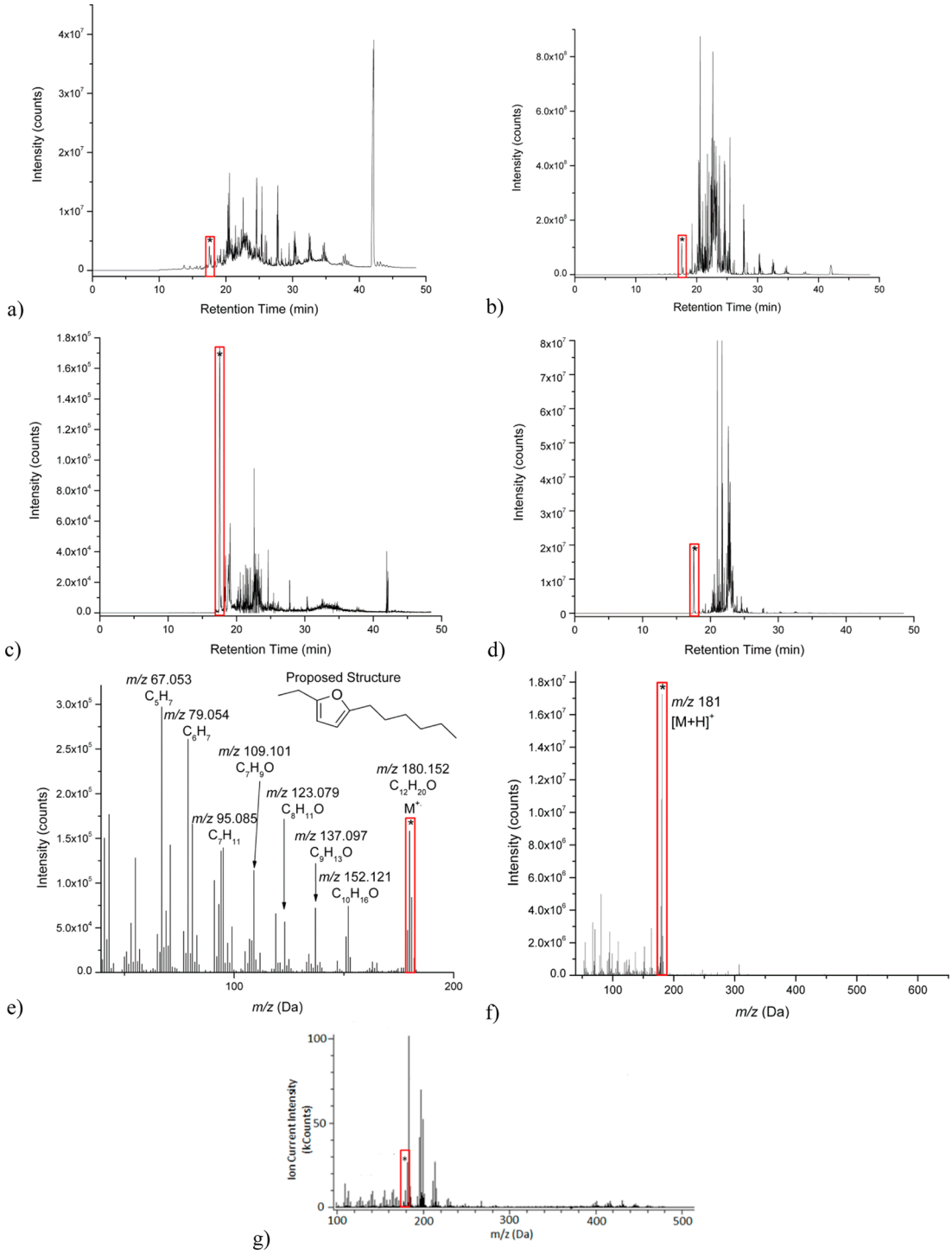

Figure 1. (a) Total ion chromatogram (EI-MS) of *n*-dodecane SOA produced under low-NO conditions with ammonium sulfate seed aerosol. The starred peak at 17.5 min corresponds to the target analyte with a molecular weight of 180 amu. (b) Total ion chromatogram (CI-MS) of *n*-dodecane SOA produced under low-NO conditions. The starred peak at 17.5 min corresponds to the target analyte with a molecular weight of 180 amu. (c) Extracted ion chromatogram (EI-MS) for m/z 180. The starred peak at 17.5 min corresponds to the target analyte with a molecular weight of 180 amu. (d) Extracted ion chromatogram (CI-MS) for m/z 180. The starred peak at 17.5 min corresponds to the target analyte with a molecular weight of 180 amu. (e) Electron impact mass spectrum at 17.5 min, with m/z values labeled from the high-resolution GC/ToF-MS analysis, along with assigned fragment formulas. (f) Chemical ionization mass spectrum at 17.5 min, with methanol as the reagent gas. (g) (+)-DART mass spectrum of *n*-dodecane SOA produced under low-NO conditions with ammonium sulfate seed aerosol. The starred peak corresponds to the target analyte with a molecular weight of 180 amu.

therefore, hydroxycarbonyl formation and carboxylic acid formation appear along the same line on a van Krevelen diagram.

Analysis of SOA by GC/MS. Filter extracts were analyzed by a Varian Saturn 2200 gas chromatograph (GC) ion trap mass spectrometer. The GC was equipped with an autosampler, a programmed temperature vaporization (PTV) injector

(Varian 1079) lined with a deactivated glass single-gooseneck liner with a deactivated glass frit (Restek, Sky, 3.4 mm ID), and a DB5-MSUI column (0.25 μm × 0.25 mm × 30 m). The PTV inlet temperature program was (i) 45 °C for 0.50 min, (ii) 180 °C min^{-1} to 300 °C, and (iii) hold at 300 °C for 46.58 min. The oven temperature program was (i) 65 °C for 10 min, (ii) 10 °C min^{-1} to final temperature of 300 °C, and (iii) 300 °C for 15 min. Electron impact and chemical ionization (CI) mass spectra were collected for each sample. The GC/CI-MS analysis was conducted with methanol as the reagent gas, generating protonated analyte species ($[M + H]^+$). These protonated species are not stable and dehydrate to form $[M + H - nH_2O]^+$. Additional analysis by GC/CI-MS/MS using methanol as the reagent gas was conducted to obtain additional structural information for compounds detected in CI mode. Additional discussion of standards analysis and measures taken to minimize method artifacts is provided in the Supporting Information.

Samples were also analyzed on a Waters GCT Premier in electron impact (EI) ionization mode. The GCT Premier combines an Agilent 6890N GC with a Waters orthogonal acceleration time-of-flight mass spectrometer (resolution 7000 fwhm). The GC was equipped with an autosampler (Agilent 7683), a split/splitless injector held at 275 °C and lined with a deactivated glass single-gooseneck liner with a deactivated glass wool plug (Restek, Sky, 4.0 mm ID), and a DB5-MS column (0.25 μm × 0.25 mm × 30 m). The oven temperature program was (i) 65 °C for 10 min, (ii) 10 °C min^{-1} to final temperature of 300 °C, and (iii) 300 °C for 15 min. Continuous introduction of perfluorotributylamine (PFTBA) to the ion source enabled accurate mass determination. Postprocessing of centroid mass spectra was carried out by linear interpolation between PFTBA peaks on either side of the analyte peak of interest.

The GC/MS data set comprises unit-mass resolution data acquired in both EI and methanol CI mode on the Varian Saturn GC/IT-MS and high-resolution data acquired in EI mode on the Waters GCT Premier. By using nearly identical temperature programs and identical columns, compounds were linked across ionization modes and instruments by retention time. A database was assembled of retention time and mass spectral data (ions formed under CI, EI-MS fragments, and molecular ions) for all samples tested. Through these correlations of molecular responses to the different ionization conditions and the use of high-resolution mass spectral data, molecular formulas were obtained using the elemental composition tool in MassLynx (Waters).

SOA samples generated under high- and low-NO conditions with ammonium sulfate seed were analyzed by high-resolution mass spectrometry with positive mode DART ionization (DART-MS). For DART-MS data, all mass spectral peaks over 1% relative intensity (approximately 1000 counts, signal-to-noise ratio ≈7) were included in the analysis. Assignments were made by choosing the minimum error for a formula that fits within the expected range of elemental compositions (C_1–C_{50}, H_1–H_{100}, O_0–O_{50}, N_0–N_5); the mass tolerance was 15 ppm. The DART-MS analysis was complemented by adding the dimension of chromatographic separation (GC/MS) with its sensitivity to structural differences. Chromatograms with unit-mass resolution electron impact and chemical ionization, as well as high mass resolution electron impact mass spectral data, were acquired for each sample. Chromatographic peak intensity was judged relative to the most intense peak present, and all chromatographic peaks over 5% relative intensity were included in the analysis.

■ RESULTS AND DISCUSSION

Chromatographic retention times were used as identifiers for compounds in GC/EI-MS (high- and unit-mass resolution) and GC/CI-MS data. GC/CI-MS peaks were paired by retention time to GC/EI-MS data acquired on the same instrument. Retention times were repeatable to ±0.01 min between chromatographic runs. Retention time indexing enabled the linking of molecular weight (obtained from the measured $[M + H]^+$) to the fragmentation pattern produced by electron impact ionization. $[M + H]^+$ unit mass values were used in conjunction with the DART-MS data to identify intact molecules outside of GC/MS analysis and to obtain molecular formulas from the high-resolution DART mass spectra. Figure 1 shows the progression of data analysis from a total ion chromatogram, which is composed of the signal of all ions as a function of retention time, for both EI- and CI-MS (Figure 1a,b), to an extracted ion chromatogram (Figure 1c,d), which targets a specific ion's signal as a function of retention time, to the mass spectrum of a compound at a specific time point (Figure 1e,f), representing a single compound. The DART mass spectrum for the same sample is depicted in Figure 1g.

Interpretation of GC/EI-MS Data. Unit-mass resolution GC/EI-MS data were linked by retention time to high-mass resolution GC/EI-MS data. The high-resolution mass spectra were the combination of the analyte and the mass calibrant, PFTBA, so the unit-mass resolution EI mass spectra were used as a reference to identify analyte peaks. The accurate masses of ions were converted to formulas through the use of Waters' Mass Lynx software. Fragmentation patterns were interpreted for structural information with the assistance of the National Institute of Standards and Technology programs MS Search and MS Interpreter.

Interpretation of GC/CI-MS Data. Methanol CI mass spectra with a pattern of peaks spaced by 18 Da were observed for many chromatographic peaks. These losses of water masses are explained as the result of dehydration reactions arising from the protonation of a hydroxylated compound; the peaks then represent $[M + H]^+$ ions and, in the case of polyhydroxylated compounds, $[M + H - nH_2O]^+$ ions. An example mass spectrum that demonstrates the dehydration that can occur when a polyhydroxylated compound undergoes chemical ionization is included in the Supporting Information.

Interpretation of DART Mass Spectra. Positive mode DART ionization uses ambient gases to execute proton transfer or form ion adducts with analyte molecules. Accurate mass measurements allowed the determination of ion formulas, and interpretation of the ion's identity as a proton, water, or ammonium adduct was done by interpreting MS/MS data from the Caltech mini-DART coupled to a Thermo LTQ ion trap mass spectrometer and by evaluating the most reasonable structure from a given formula derived from accurate mass measurements made with the JEOL AccuToF DART. $[M + H]^+$ and $[M + H - nH_2O]^+$ m/z values from DART-MS were correlated with GC/CI-MS values and thereby linked with their chromatographic retention times and electron impact mass spectra acquired with unit-mass and high resolution. Multiple occurrences of $[M + H]^+$ and $[M + H - nH_2O]^+$ m/z values at different retention times were interpreted as different structural isomers (see Figure 1c).

Reactive DART-MS methods were used with the Caltech mini-DART to differentiate nitrates, imines, and hydroperoxide-ammonium adducts. The flexible ionizer configuration allowed for the inclusion into the DART gas stream of 1,4,7,10,13,16-hexaoxacyclooctadecane (abbrev. 18-crown-6), a reagent that strongly complexes with primary amines. An important analytical goal was to differentiate ammonium ion adducts from imine or nitrate compounds by monitoring the decrease and disappearance of even m/z compounds from the mass spectrum upon the introduction of 18-crown-6. The decline of ammonium ion adducts with peroxides in the presence of 18-crown-6 is caused by the more favorable formation of 18-crown-6 ammonium ion adducts. Proton adducts of peroxides are then detected once the ammonium ion-peroxide adducts are not produced in high abundance. Spectra that illustrate this method of analysis are provided in the Supporting Information.

SOA Composition. The experiments were targeted at exploring the effects of structure (cyclic versus linear alkane) on SOA composition, and for each structure, the effects of the RO_2 + HO_2 pathway (low NO) versus the RO_2 + NO pathway (high NO). For the *n*-dodecane system, the additional effects of relative humidity and seed type on SOA composition were investigated.

***n*-Dodecane SOA Composition.** *n-Dodecane Low-NO SOA Composition.* *n*-Dodecane, when oxidized in the RO_2 + HO_2 regime, forms hydroperoxides and hydroxyl- and carbonyl-bearing compounds (Figure 2).[28,32] These functional additions can occur sequentially on the full C_{12} backbone or on smaller carbon chains if fragmentation reactions are occurring. Products of sufficiently low volatility appear in the particle phase.

The dominant species in *n*-dodecane SOA under the low-NO regime are functionalized hemiacetals and peroxyhemiacetals, which together constitute over 98% of the assigned SOA mass (Figure 2a). These compounds form from particle-phase reactions that are traditionally considered to be acid-catalyzed; we propose that ammonium ions from the seed are involved because of their abundance and activity (Scheme 1). Under ~4% RH conditions, ammonium sulfate seed is minimally hydrated with physisorbed monolayers of water. Ammonium sulfate seed has been shown for other hydrocarbon systems to promote oligomer formation under dry conditions from pathways that are traditionally acid-catalyzed.[3,4,63] The presence of these oligomers is consistent with the activity of an acid catalyst, but we cannot unequivocally establish that ammonium ions and surface monolayers of water are responsible for the products we found.

Peroxyhemiacetals form from the reaction of an aldehyde or ketone and a hydroperoxide group (Scheme 2).[25] The formation of oligomeric species such as peroxyhemiacetals has been shown via kinetic gas-particle modeling to be consistent with the observed evolution of the size distribution of alkane SOA.[36] Hydroperoxides and alcohols are ~8 orders of magnitude lower in relative concentration than hemiacetals and ~6 orders of magnitude lower than peroxyhemiacetals; this suggests that oligomer formation is favored. The mean molecular weight for *n*-dodecane low-NO SOA was calculated to be 429.01 g mol^{-1} (Table 4), reiterating the important role of oligomeric species in *n*-alkane SOA formation.

Hydroxycarbonyls are the most abundant monomeric species, a finding that is consistent with previous alkane studies (Figure 2a).[28,32,37,39] These hydroxycarbonyls, when substituted in a 1,4 configuration, can undergo intramolecular cyclization to form cyclic hemiacetals, which in the presence of a suitable acid catalyst are dehydrated to form dihydrofurans (Scheme 3).[37,64,65] If these dihydrofurans carry additional hydroxyl groups on the ring, they may undergo an additional dehydration step to form a furan. Both dihydrofurans and furans were detected in this study, with dihydrofurans being more prevalent than furans in the particle phase.

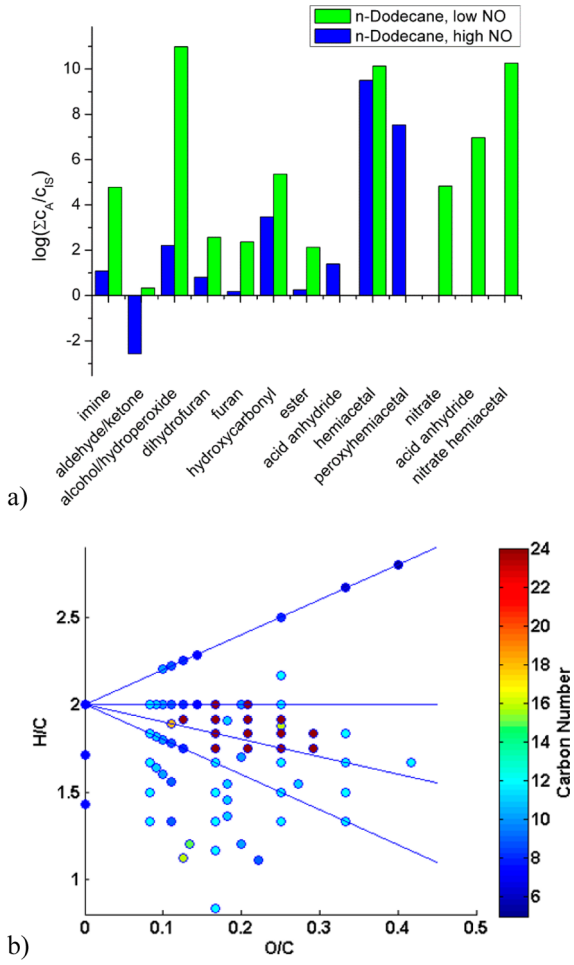

Figure 2. (a) *n*-Dodecane SOA composition under dry, low- and high-NO conditions with $(NH_4)_2SO_4$ seed. (b) Van Krevelen diagram for *n*-dodecane SOA produced under dry, low-NO conditions with $(NH_4)_2SO_4$ seed. A slope of 2 can be interpreted to represent hydration reactions. A slope of 0 can be interpreted to represent the formation of a hydroxy or peroxy group. A slope of −1 can represent the formation of a carboxylic acid group or the addition of a hydroxy group and a carbonyl group on the same molecule. A slope of −2 can represent the addition of a carbonyl group.

A carbonyl can be converted to an imine in the particle phase in the presence of an amine or ammonium ions and ammonia, as is the case in this study (Scheme 3).[38,66] The imine population is measured here to be larger than the purely aldehyde and ketone components, suggesting that the majority of ketones and aldehydes are converted to imines. The carbonyl population upon which the imine formation process draws includes hydroxycarbonyls, ketones, aldehydes, and functionalized furans and dihydrofurans.

The van Krevelen diagram for *n*-dodecane low-NO SOA (Figure 2b) indicates that hydration reactions and the formation of alcohols, peroxides, carbonyls, and hydroxycar-

Scheme 1. Proposed Mechanism for the Formation of Hemiacetals (m/z 431) in Dodecane SOA Formed under Low-NO Conditions[a]

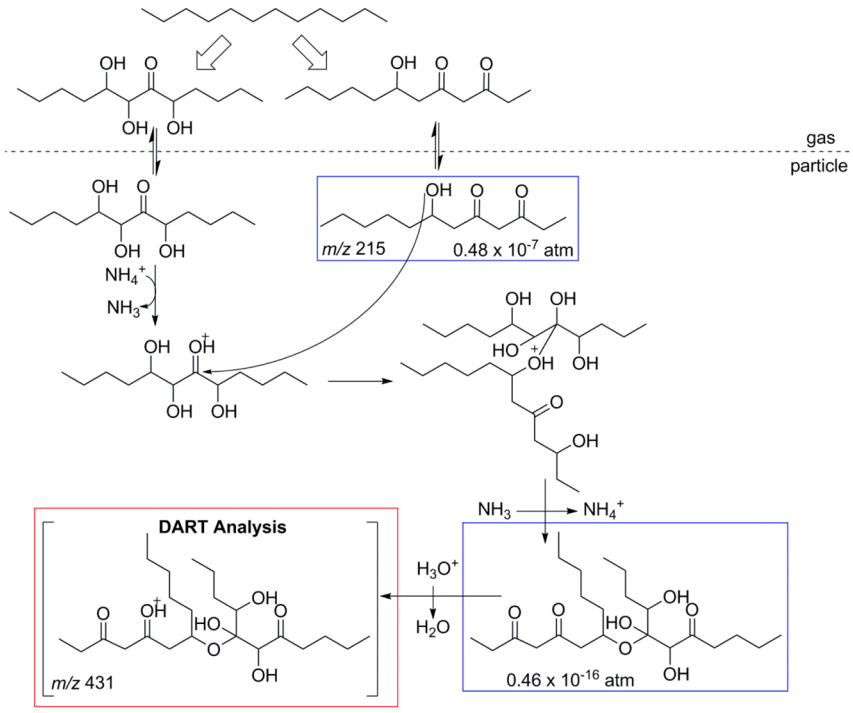

[a]Large arrows indicate several gas-phase photooxidation steps. Proposed structures are boxed in blue. Ion clusters as measured by mass spectrometry are boxed in red. Vapor pressures are estimated by EVAPORATION.[43]

Scheme 2. Proposed Mechanism for the Formation of Peroxyhemiacetals (m/z 432) in Dodecane SOA under Low-NO Conditions[a]

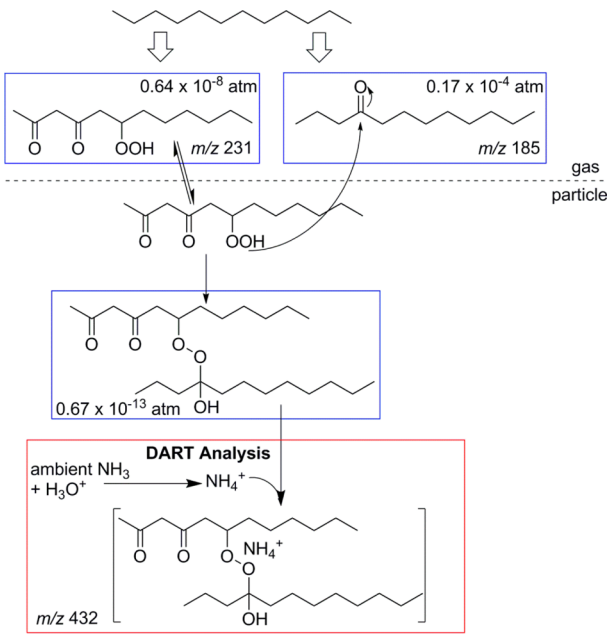

[a]Large arrows indicate several gas-phase photooxidation steps. Proposed structures are boxed in blue. Ion clusters as measured by mass spectrometry are boxed in red. Vapor pressures are estimated by EVAPORATION.[43]

bonyls are all key processes in directing the chemical composition. Hydration processes occur for unsaturated photooxidation products, such as furans and dihydrofurans, and would most likely occur at a hydrated surface layer of a particle or the chamber wall. At <4% RH, the gas phase would be an unlikely place for hydration to occur. The majority of data points trend in the space between the ketone/aldehyde slope and the alcohol/peroxide slope; this space is bisected by the hydroxycarbonyl slope, which is consistent with the importance of hydroxycarbonyl-bearing compounds in the quantitative analysis.

Some of the compounds measured here are estimated to have relatively high volatility, a property that is consistent with facile DART-MS detection. It is possible that these relatively high volatility compounds are, in fact, present at a concentration lower than that of the C_{12} products but undergo more facile detection by DART-MS, even though their concentration may be below the effective method limit of detection for extraction-GC/MS analysis. Shiraiwa et al.[36] suggest that particle growth in the dodecane low-NO system is driven by oligomerization and that the resultant particles are semisolid in phase. That reasoning is consistent with the presence of these products as oligomers that are destabilized upon ionization and are measured as their monomers; a semisolid nature of the aerosol phase possibly explains why these relatively volatile compounds could remain trapped in the particle phase as well. Additional explanation for the apparent discrepancy could also be found in the negligible sample preparation required for DART-MS analysis versus the extensive sample preparation and elevated temperatures necessary for GC/MS analysis. Both sample preparation and elevated temperature can lead to losses of sensitive or thermally labile compounds in GC/MS; by comparison, DART-MS provides a more comprehensive breadth of analysis by

Table 4. Alkane SOA Mean Molecular Weights and Mean O:C and H:C Ratios

parent VOC	NO conditions	% speciation	mean molecular weight of SOA (g mol^{-1})	mean atomic O:C ratio	mean atomic H:C ratio
n-dodecane	low	92	429.01	0.25	1.93
	high	95	495.33	0.47	2.07
cyclododecane	low	99	384.52	0.18	1.61
	high	99	458.38	0.35	1.72
hexylcyclohexane	low	95	310.49	1.09	1.53
	high	98	418.06	0.30	1.65

Scheme 3. Proposed Mechanism for Formation of Furan (*m/z* 209) and Imine (*m/z* 208) Species in *n*-Dodecane SOA Generated under Low-NO Conditions[a]

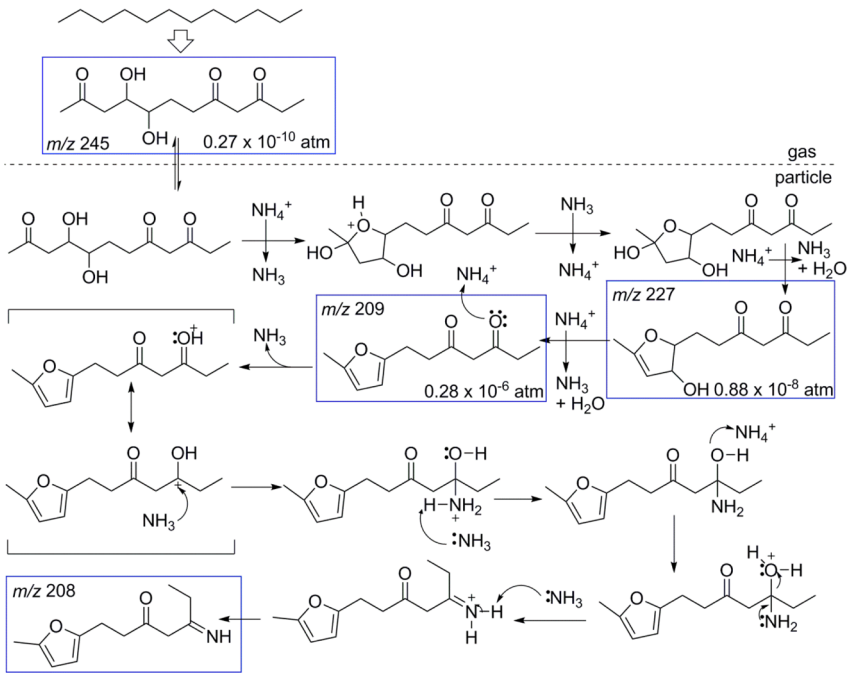

[a]Vapor pressures are estimated by EVAPORATION.[43]

preserving even highly unstable and reactive molecules for detection.

n-Dodecane High-NO SOA Composition. Under dominant RO_2 + NO gas-phase chemistry, the photooxidation proceeds through the formation of alkoxy radicals, which undergo decomposition to aldehydes or isomerization to form alcohols.[23,24,27] Further oxidation of aldehydes by ozone present under high-NO conditions produces carboxylic acids, facilitating the production of esters and serving as a reaction catalyst.[67] Organonitrates are also expected products in the particle phase.[27] Expected oligomers, given these starting materials and conditions, are esters and ethers carrying other pendant groups as well as carboxylic acid anhydrides.

Figure 2a gives an overview of the chemical composition of *n*-dodecane SOA from high-NO conditions. The dominant species are alcohols, hemiacetals, nitrate-bearing hemiacetals, and acid anhydrides. The majority of monomers are alcohols, hydroxycarbonyls, imines, and nitrates, with a smaller proportion of dihydrofurans, furans, and ketones present. Imines, dihydrofurans, and furans result from particle-phase chemistry, as do hemiacetals and acid anhydrides (Schemes 2−4). The van Krevelen diagram (Figure 3) shows the importance of oxygenated smaller carbon chain compounds as well as the presence of highly substituted alcoholic species. The atomic O:C ratio reaches 1 in this system, as opposed to the atomic O:C ratio of 0.5 under low-NO conditions. Sub-C_{12} compounds that result from fragmentation comprise aldehydes and hydroxycarbonyls, which have vapor pressures higher than those of compounds normally attributed to exist in the particle phase. Shiraiwa et al.[36] predict a semisolid particle phase for dodecane low-NO SOA, which implies that higher volatility material can be trapped between layers of less volatile material during the particle accretion process.

The presence of a series of C_{13} compounds with high degrees of oxygenation (O:C of 0.38−0.62) can be explained as the formation of C_{13} oligomers from a combination of sub-C_{12} hydroxycarbonyl compounds. These monomers are multifunctional, including β-hydroxycarbonyls, and therefore could combine to form oligomers via aldol condensation or ether or ester formation. Aldol condensation has been found to occur in the presence of amines, so ammonia from the seed could potentially serve to enable the condensation of aldehydes and β-hydroxycarbonyls in the particle phase.[68] Additional compounds with backbones $>C_{12}$ but $<C_{24}$ are also consistent with oligomerization of dissimilar monomers.

The oligomers formed under high-NO conditions are predominantly hemiacetals, nitrate hemiacetals, with smaller concentrations of carboxylic acid anhydrides and esters (Scheme 4). An ester would form via an acid group from an aldehyde, which is known to form through the chain

Scheme 4. Proposed Mechanism for the Formation of Hemiacetals (m/z 458) in Dodecane SOA Formed under High-NO Conditions[a]

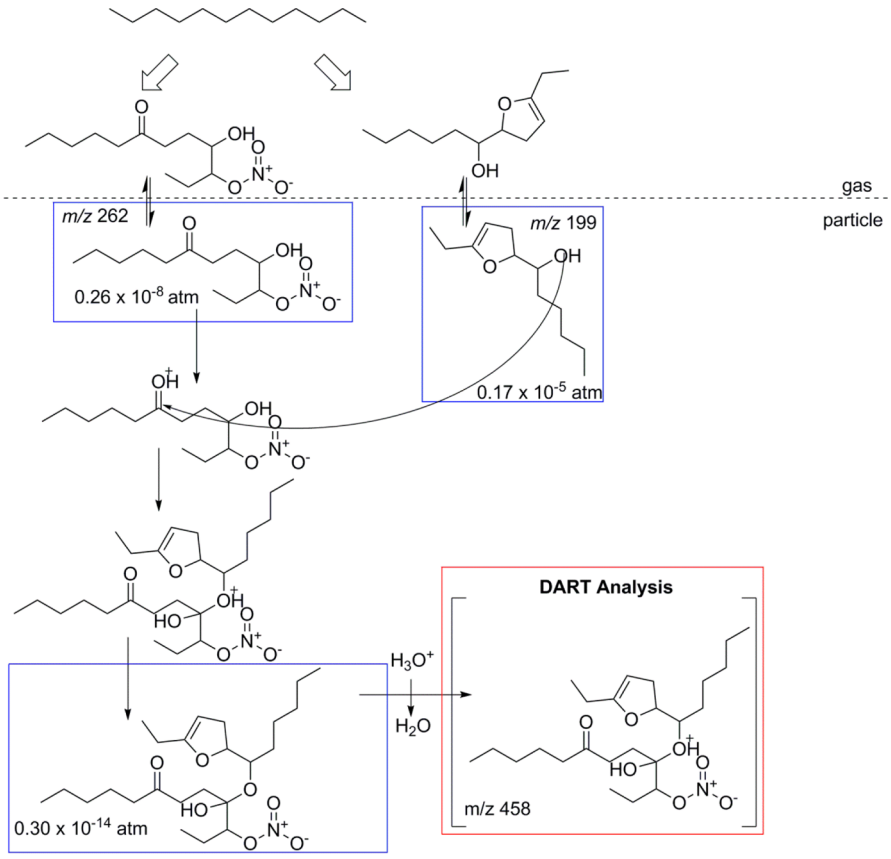

[a]Large arrows indicate several gas-phase photooxidation steps. Proposed structures are boxed in blue. Ion clusters as measured by mass spectrometry are indicated in the red box. Vapor pressures are estimated by EVAPORATION.[43]

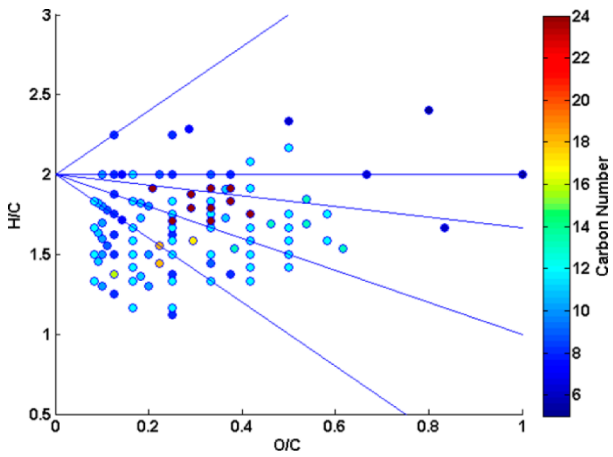

Figure 3. Van Krevelen diagram for n-dodecane SOA produced under dry, high-NO conditions with $(NH_4)_2SO_4$ seed. A slope of 2 can be interpreted to represent hydration reactions. A slope of 0 can be interpreted to represent the formation of a hydroxy or peroxy group. A slope of −1 can represent the formation of a carboxylic acid group or the addition of a hydroxy group and a carbonyl group on the same molecule. A slope of −2 can represent the addition of a carbonyl group. A slope of −1/3 can represent the addition of a nitrate group.

Scheme 5. Proposed Mechanism for the Formation of Carboxylic Acids in the Presence of Ozone under High-NO Conditions, Following Ziemann et al. 2005[67]

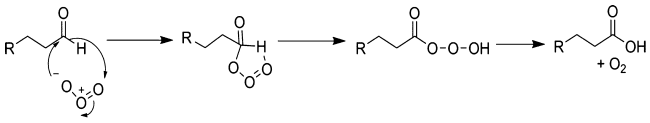

fragmentation pathway. Aldehyde ozonolysis under high-NO conditions is known to produce carboxylic acids (Scheme 5).[69] On the basis of the retention of all 12 carbons by both monomer units, the C_{24} oligomers are likely linked through hemiacetal groups. Lim and Ziemann[23,24,52] have proposed the particle-phase formation of cyclic hemiacetals or full acetals. Hemiacetals, including those bearing nitrate groups, are present at ∼8 orders of magnitude higher concentrations than esters. Hemiacetals are much more abundant under high-NO conditions for n-dodecane than under low-NO conditions; this is consistent with the large increase in alcohol formation due to RO_2 + NO reactions.

It is also important to note that the organic aerosol loading increased by a factor of 2.3 from the low-NO to the high-NO case (Table 2) and that the mean molecular weight increased from 429.01 to 495.33 g mol^{-1} (Table 4). The production of secondary nitrates under these conditions, along with drastically increased ether formation from the large alcohol population, is the simplest route to this increase in organic aerosol production and increase in compounds with high molecular weights. In comparison to hexylcyclohexane and cyclododecane, the linear structure of n-dodecane offers no tertiary sites and ring sites for

nitration; thus, the volume concentration enhancement is less than for the other structures.

Cyclododecane SOA Composition. *Cyclododecane Low-NO SOA Composition.* Cyclododecane low-NO SOA is dominated by ethers and peroxyhemiacetals and contains contributions of hydroxycarbonyls, hydroperoxides, and alcohols that are more significant than those in *n*-dodecane low-NO SOA. The cyclododecane product distribution under low-NO conditions clearly exhibits both functionalization and fragmentation (Figure 4). The stable molecules that result from fragmentation of cyclododecane are highly oxidized, especially when compared to the *n*-dodecane products.

Yee et al.[29] report that cyclododecane undergoes two characteristic periods of chemical development: the early formation of hydroperoxides, hydroxy hydroperoxides, and dicarbonyl hydroperoxides, followed by the formation of ring-opened products, which include an aldehyde group. The rapid addition of oxygenated groups observed by Yee et al.,[29] in conjunction with aldehyde formation associated with ring-opening, is consistent with the observations here of elevated functionality and fragmentation of these highly oxidized structures. The atomic O:C ratio for cyclododecane extends to 1.25, but the H:C ratio indicates the compound remains saturated, reflecting the importance of hydroperoxyl and hydroxyl groups in the oxidation of cyclododecane; for *n*-dodecane, the atomic O:C ratio did not exceed 0.45.

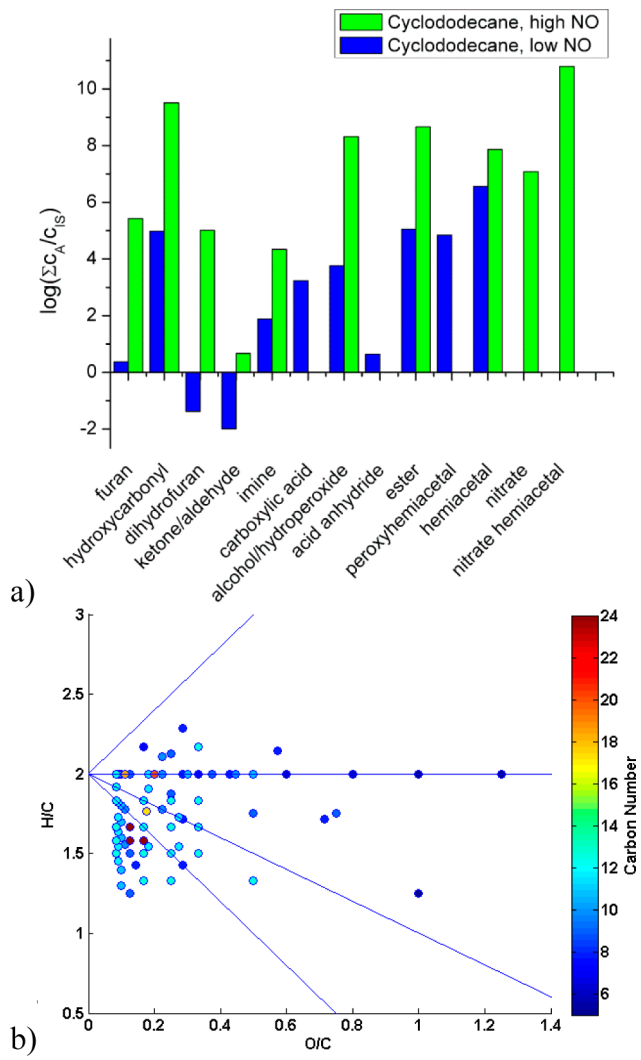

Figure 4. (a) Composition of cyclododecane SOA produced under dry, low- and high-NO conditions, with $(NH_4)_2SO_4$ seed. (b) Van Krevelen diagram for cyclododecane SOA produced under dry, low-NO conditions, with $(NH_4)_2SO_4$ seed. A slope of 2 can be interpreted to represent hydration reactions. A slope of 0 can be interpreted to represent the formation of a hydroxy or peroxy group. A slope of −1 can represent the formation of a carboxylic acid group or the addition of a hydroxy group and a carbonyl group on the same molecule. A slope of −2 can represent the addition of a carbonyl group.

The C_{12} and sub-C_{12} compounds (Figure 4) constitute a mixture of hydroperoxides, hydroxy hydroperoxides, carbonyl hydroperoxides, carbonyl hydroxy hydroperoxides, hydroxycarbonyls, ketones, and aldehydes. These compounds are the building blocks of the oligomeric species that dominate the aerosol composition, and they also are responsible for increasing the atomic O:C ratio range occupied by cyclododecane SOA components. They constitute a sufficient amount of the SOA mass to also decrease the mean molecular weight as compared to that of *n*-dodecane low-NO SOA (Table 4).

Imines are present at a comparable concentration in cyclododecane and *n*-dodecane low-NO SOA. This result is expected because the total relative amounts of carbonyl-bearing species are approximately equivalent and ammonia from the aerosol seed is abundant and not limiting in either case.

Oligomers in cyclododecane low-NO SOA are, in decreasing order by concentration, hemiacetals, esters, peroxyhemiacetals, and carboxylic acid anhydrides. The contribution of esters in this system is 5 orders of magnitude higher than that for *n*-dodecane, and this can be attributed to the ring structure breaking to form C_{12} dialdehydes, which can react with OH radicals to form carboxylic acids. The presence of hemiacetals, which arise through an acid-catalyzed reaction, suggests the sufficiency of the ammonium ion and carboxylic acid populations to serve as catalysts for other acid-catalyzed processes (Scheme 6). These oligomeric species, combined with the smaller-chain but highly oxygenated compounds, produce a mean molecular weight of 384.52 g mol^{-1}.

Cyclododecane High-NO SOA Composition. Cyclododecane SOA produced under high-NO conditions is primarily composed of ethers with or without pendant nitrate groups, esters, hydroxycarbonyls, alcohols, and nitrates (Figure 4a). The majority of the aerosol is formed of oligomeric species, particularly hemiacetals (combined relative concentration of ~10[19]). The mean molecular weight for this system is 458.48 g mol^{-1}, which reflects the large contributions of oligomers and increased molecular weights from nitration.

Cyclododecane oxidized under high-NO conditions shows the same propensity toward extensive functionalization and fragmentation that opens the ring or breaks the C_{12} backbone as under low-NO (Figure 5). The high-NO composition is characterized by an abundance of nitrated compounds that are also extensively oxygenated. Lim and Ziemann[22,24,70] note that an alkoxy radical formed on a cyclododecane ring is prone to rapid decomposition compared with the linear form because of high ring strain and suggested that a cyclic alkyl nitrate may be more volatile than a linear alkyl nitrate because the nitrate is never in a terminal chain position. If the vapor pressures of the cyclododecane nitrates were sufficiently high, they would remain in the gas phase and continue to undergo gas-phase OH oxidation, generating these highly functionalized compounds, including the dinitrate. Cyclododecane reaches a

Scheme 6. Proposed Mechanism for the Formation of Hemiacetals (*m/z* 391) in Cyclododecane SOA under Low-NO Conditions[a]

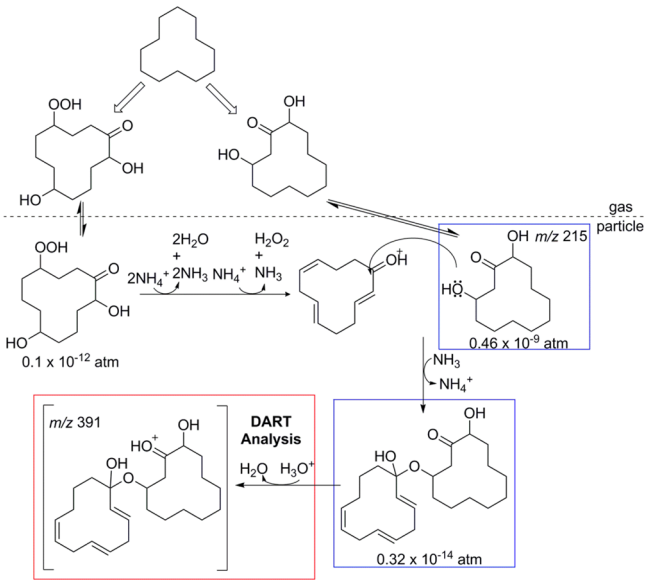

[a]Large arrows indicate several gas-phase photooxidation steps. Proposed structures are boxed in blue. Ion clusters as measured by mass spectrometry are indicated in the red box. Vapor pressure calculated for ether was performed for the proxy compound without carbon−carbon double bonds. Vapor pressures are estimated by EVAPORATION.[43]

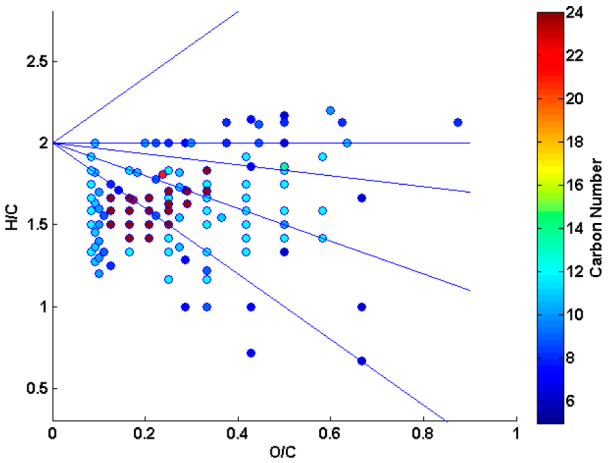

Figure 5. Van Krevelen diagram for cyclododecane SOA produced under dry, high-NO conditions, with $(NH_4)_2SO_4$ seed. A slope of 2 can be interpreted to represent hydration reactions. A slope of 0 can be interpreted to represent the formation of a hydroxy or peroxy group. A slope of −1 can represent the formation of a carboxylic acid group or the addition of a hydroxy group and a carbonyl group on the same molecule. A slope of −2 can represent the addition of a carbonyl group. A slope of −1/3 can represent the addition of a nitrate group.

comparable maximum atomic O:C as *n*-dodecane under high-NO conditions (Figures 4b and 5). The product distribution density is greater toward the carboxylic acid and hydroxycarbonyl slope and the carbonyl slope, which is consistent with past studies.[22,24] From the van Krevelen diagram representation, the production of hydroxycarbonyls, dihydrofurans, and furans is greatly increased under high-NO conditions as compared to that under low-NO conditions. Furans and dihydrofurans, along with their cyclic hemiacetal precursor, carry side-chains with a variety of degrees of functionalization by hydroxyl, ketone, and nitrate groups.

Cyclododecane shows a far greater propensity toward oligomer generation under high-NO conditions than under low-NO conditions. Nitrate hemiacetals are the dominant species, and nitrates are the third most abundant monomeric species in the particle phase. These oligomers comprise cyclic, straight-chain, and furan monomer units that carry additional oxygenated groups as well as imine groups. The organic aerosol volume concentration for cyclododecane under high-NO conditions was found to be a factor of 5 higher than that under low-NO conditions (Table 2). The enhancement of volume concentration and high mean molecular weight (Table 4) under high-NO conditions suggests the importance of nitrate groups to decreasing oxidation product volatility and increasing partitioning to the particle phase.

Hexylcyclohexane SOA Composition. *Hexylcyclohexane Low-NO SOA Composition.* Hexylcyclohexane SOA generated under low-NO conditions is composed predominantly of hydroperoxides, peroxyhemiacetals, hemiacetals, and hydroxycarbonyls (Figure 6a); this composition spectrum is in contrast to those of *n*-dodecane and cyclododecane, with particle-phase compositions dominated by oligomeric species. Some of the hydroxycarbonyls and ketones are converted to imines, as in the other alkane systems.

The concentration of hydroxycarbonyls in hexylcyclohexane SOA is a factor of 10^3 higher than in *n*-dodecane and cyclododecane aerosol. The imine concentration for hexylcyclohexane SOA is a factor of 10^4 higher than that for *n*-dodecane and cyclododecane aerosol, as well. The increase in imine concentration can be attributed to the larger concentration of carbonyl compounds available to be converted into imines through reaction with ammonium in the seed aerosol.

The hexylcyclohexane low-NO SOA clearly reflects the gas-phase oxidation mechanism. The sub-C_{12} products are either ring-retaining C_6 or from the *n*-hexyl chain, which has been cleaved from the cyclohexane ring. Cleavage of the cyclohexyl ring from the *n*-hexyl chain can occur through decomposition of an alkoxy radical formed at the tertiary carbon site. Radical formation at the tertiary site is favored for its stability. *n*-Hexane and cyclohexane products can be differentiated by the additional degree of unsaturation of cyclohexane due to its structure. The *n*-hexyl chain can be further fragmented along with being substituted with carbonyl, hydroperoxide, or hydroxyl groups. This substitution pattern upon these two frameworks can be seen in the pattern visible in the van Krevelen diagram (Figure 6b).

Oligomeric species feature prominently in the hexylcyclohexane system, particularly peroxyhemiacetals (Scheme 7) and hemiacetals, but they are not the most abundant molecules in the resulting SOA. The peroxyhemiacetal concentration for hexylcyclohexane is 10 times higher than that for *n*-dodecane and a factor of 10^3 higher than that for cyclododecane. The concentration of hemiacetals in hexylcyclohexane low-NO SOA is equivalent to that for cyclododecane but is less than that for *n*-dodecane. The increased production of peroxyhemiacetals in hexylcyclohexane is linked with the highest concentration of hydroperoxides out of the three systems ($\sim 10^{12}$). The asymmetry of hexylcyclohexane produces more structurally distinctive compounds than either *n*-dodecane or cyclododecane for the same set of chemical reactions. The tertiary carbon in hexylcyclohexane becomes the most stable peroxy

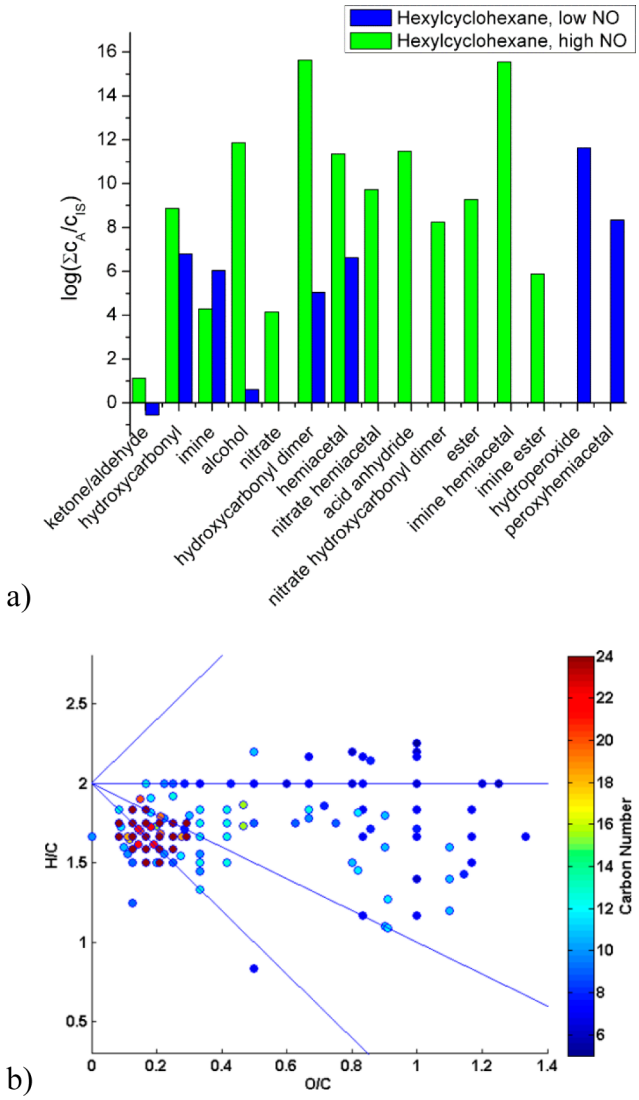

Figure 6. (a) Composition of hexylcyclohexane SOA produced under dry, low- and high-NO conditions, with $(NH_4)_2SO_4$ seed. (b) Van Krevelen diagram for hexylcyclohexane SOA produced under dry, low-NO conditions, with $(NH_4)_2SO_4$ seed. A slope of 2 can be interpreted to represent hydration reactions. A slope of 0 can be interpreted to represent the formation of a hydroxy or peroxy group. A slope of −1 can represent the formation of a carboxylic acid group or the addition of a hydroxy group and a carbonyl group on the same molecule. A slope of −2 can represent the addition of a carbonyl group.

Scheme 7. Proposed Mechanism for Formation and Detection by DART-MS of Peroxyhemiacetals (*m/z* 412) in Hexylcyclohexane SOA Generated under Low-NO Conditions[a]

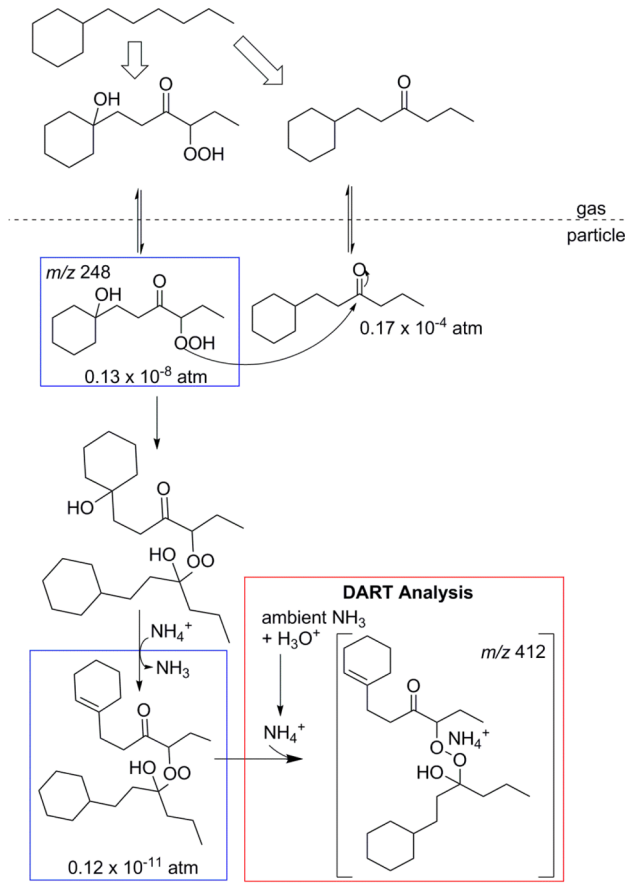

[a]Large arrows indicate several gas-phase photooxidation steps. Proposed structures are boxed in blue. Ion clusters as measured by mass spectrometry are indicated in the red box. Vapor pressures are estimated by EVAPORATION.[43]

radical out of these three alkanes, leading to a more enduring contribution to SOA mass. The mean molecular weight, 310.49 g mol^{-1}, is the lowest among the three parent structures and points to the important presence of low-volatility monomers in the particle phase (Table 4).

Hexylcyclohexane High-NO SOA Composition. Under high-NO conditions, alkoxy radicals drive the chemistry, fragmentation, functionalization, and oligomerization in hexylcyclohexane SOA formation (Figure 7). The uniquely stable cyclohexyl ring allows the formation of C_6 species that can be fully substituted with hydroxyl groups. A C_6 nitrate is also detected, but it is likely on the straight-chain or at the tertiary site that serves as the juncture of the cyclohexane ring and *n*-hexyl chain, based on Lim and Ziemann's conclusion that cyclic alkyl nitrates are more volatile than straight-chain alkyl nitrates.[23,70] Nitrates are observed from C_5 to C_{12}, most of which do not bear additional oxygen atoms. The lack of additional oxygenation suggests that these nitrates condense into the particle phase directly and do not undergo additional cycles of oxidation. The variance in chain length suggests alkyl chain cleavage due to alkoxy radical formation and decomposition into an aldehyde and an alkyl radical, which becomes a RO_2 radical that reacts with NO. These smaller RO_2 are less prone to form a nitrate in RO_2 + NO.

Hexylcyclohexane SOA produced under high-NO contained an abundance of oligomeric compounds: hydroxycarbonyl dimers, with and without pendant nitrate groups, formed through aldol condensation; hemiacetals with and without pendant nitrate or imine groups; and esters with and without pendant imine groups (Figure 6a). Esters were more abundant in this system than for any of the other parent structures, likely because of the ease of aldehyde and carboxylic acid formation through the oxidation of *n*-hexyl chain cleavage products and the presence of ozone due to the high-NO conditions. Hemiacetals and aldol condensation products are present in the particle-phase because of the existence of alcohols and *β*-hydroxycarbonyls (Scheme 8). The pronounced presence of imines in the oligomer products is related to the large number of carbonyl-bearing compounds, as seen in the van Krevelen

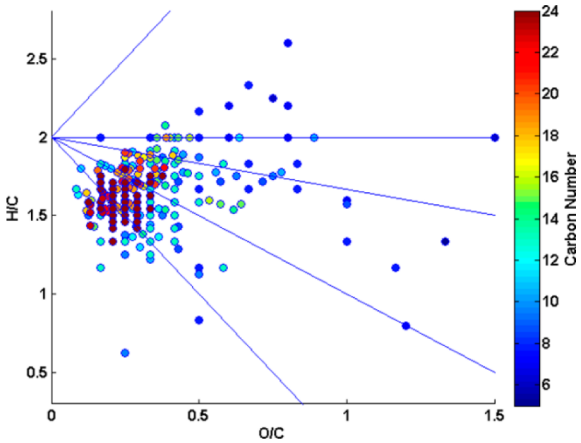

Figure 7. Van Krevelen diagram for hexylcyclohexane SOA produced under dry, high-NO conditions, with $(NH_4)_2SO_4$ seed. A slope of 2 can be interpreted to represent hydration reactions. A slope of 0 can be interpreted to represent the formation of a hydroxy or peroxy group. A slope of −1 can represent the formation of a carboxylic acid group or the addition of a hydroxy group and a carbonyl group on the same molecule. A slope of −2 can represent the addition of a carbonyl group. A slope of −1/3 can represent the addition of a nitrate group.

diagram (Figure 7). Dominant trends occur along the hydroxycarbonyl slope and ketone/aldehyde slope. The maximum atomic O:C ratio for this system (1.5) is higher than for any of the other parent compounds under either NO condition.

The organic aerosol volume concentration (see Table 2) is found to increase by a factor of 2.8 from low- to high-NO conditions, an increase that can be attributed primarily to the presence of nitrates in the aerosol phase. The increase in hexylcyclohexane SOA volume concentration from low- to high-NO conditions is higher than that for *n*-dodecane but less than that for cyclododecane. This trend in NO-related volume concentration increase underlies the importance of cyclic structure and increased secondary sites for the particle-phase partitioning of alkyl nitrates. The mean molecular weight of 418.06 g mol^{-1} is the largest increase in mean molecular weight in this study when going from low- to high-NO conditions for a given system (Table 4). High degrees of functionalization and oligomerization in high-NO hexylcyclohexane-derived SOA lead to its large mean molecular weight.

■ CONCLUSIONS

SOA formed in the *n*-dodecane, cyclododecane, and hexylcyclohexane systems is largely the result of particle-phase chemistry. The contribution of oligomeric compounds to alkane SOA has been reported previously (Table 1).[15,28,32] We demonstrate here the importance of peroxyhemiacetals in generating aerosol mass from alkane photooxidation under low-NO conditions and the relevance of ether formation across NO conditions. These findings underscore the importance of NO-induced chemistry and parent compound structure in

Scheme 8. Proposed Mechanism for the Formation of Hemiacetals (*m/z* 472) in Hexylcyclohexane SOA Formed under High-NO Conditions[a]

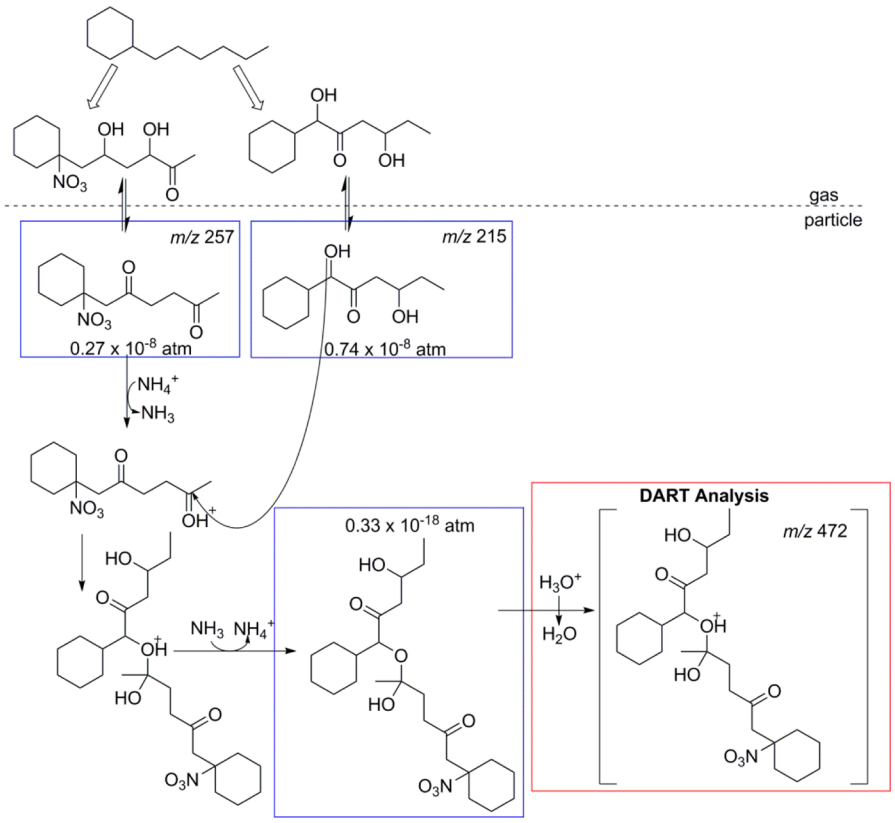

[a]Large arrows indicate several gas-phase photooxidation steps. Proposed structures are boxed in blue. Ion clusters as measured by mass spectrometry are indicated in the red box. Vapor pressures are estimated by EVAPORATION.[43]

determining the chemical structure and functionality of SOA oligomeric species. Under high-NO conditions, organic aerosol volume can vary by a factor of 2.3−5, depending on the structure of the parent C_{12} alkane. This variation in aerosol mass reflects the importance of nitrate formation in the alkane system. In addition, nitrogen incorporation from the ammonium seed aerosol into the organic component of the aerosol through the formation of imines is reported here for the three alkane systems. Imine concentration is correlated with the amount of carbonyl-bearing compounds, as expected, and is therefore an important component of alkane SOA, which is rich in ketones, aldehydes, and hydroxycarbonyls.

The complex compositional data presented here demonstrate the relevance of particle-phase chemistry in alkane-derived SOA and the importance of the ammonium ion as a source of nitrogen incorporation into organic aerosol. The data reinforce the understanding that, for long-chain alkanes, there exist a large number of oxidation products, each of which is present at a relatively low concentration. This finding is an important consideration in generating mechanisms for SOA formation that can eventually be included in atmospheric models.

■ ASSOCIATED CONTENT

Supporting Information

Additional information and example data for the DART-MS and GC/MS analytical methods; the equations to describe the weighted averaging procedure to obtain mean molecular weights; quantitative compositional data; proposed structures and calculated vapor pressures using the EVAPORATION model for *n*-dodecane, cyclododecane, and hexylcyclohexane SOA. This material is available free of charge via the Internet at http://pubs.acs.org.

■ AUTHOR INFORMATION

Corresponding Author

*E-mail: seinfeld@caltech.edu.

Present Addresses

[§]C.L.L.: 3M Environmental Laboratory, 3M Center, Building 260-05-N-17, St. Paul, MN.

[∥]L.D.Y: Environmental Science, Policy, and Management at University of California, Berkeley, CA.

Notes

The authors declare no competing financial interest.

■ ACKNOWLEDGMENTS

The authors thank Mark S. Andersen of the Jet Propulsion Laboratory and Kathleen T. Upton and Jesse L. Beauchamp of the California Institute of Technology for experimental assistance with DART-MS. This research was funded by U.S. Department of Energy Grant DE-SC 0006626 and National Science Foundation Grant AGS-1057183. K.A.S.F. acknowledges support from a Department of Defense Science, Mathematics, and Research for Transformation Fellowship.

■ REFERENCES

(1) Molina, M. J.; Ivanov, A. V.; Trakhtenberg, S.; Molina, L. T. Atmospheric Evolution of Organic Aerosol. *Geophys. Res. Lett.* **2004**, *31*, L22104.

(2) Kalberer, M.; Paulsen, D.; Sax, M.; Steinbacher, M.; Dommen, J.; Prevot, A. S. H.; Fisseha, R.; Weingartner, E.; Frankevich, V.; Zenobi, R.; et al. Identification of Polymers as Major Components of Atmospheric Organic Aerosols. *Science* **2004**, *303*, 1659−1662.

(3) Gao, S.; Ng, N. L.; Keywood, M.; Varutbangkul, V.; Bahreini, R.; Nenes, A.; He, J.; Yoo, K. Y.; Beauchamp, J. L.; Hodyss, R. P.; et al. Particle Phase Acidity and Oligomer Formation in Secondary Organic Aerosol. *Environ. Sci. Technol.* **2004**, *38*, 6582−6589.

(4) Gao, S.; Keywood, M.; Ng, N. L.; Surratt, J.; Varutbangkul, V.; Bahreini, R.; Flagan, R. C.; Seinfeld, J. H. Low-Molecular-Weight and Oligomeric Components in Secondary Organic Aerosol from the Ozonolysis of Cycloalkenes and α-Pinene. *J. Phys. Chem. A* **2004**, *108*, 10147−10164.

(5) Tolocka, M. P.; Jang, M.; Ginter, J. M.; Cox, F. J.; Kamens, R. M.; Johnston, M. V. Formation of Oligomers in Secondary Organic Aerosol. *Environ. Sci. Technol.* **2004**, *38*, 1428−1434.

(6) Loeffler, K. W.; Koehler, C. A.; Paul, N. M.; De Haan, D. O. Oligomer Formation in Evaporating Aqueous Glyoxal and Methylglyoxal Solutions. *Environ. Sci. Technol.* **2006**, *40*, 6318−6323.

(7) Baltensperger, U.; Kalberer, M.; Dommen, J.; Paulsen, D.; Alfarra, M. R.; Coe, H.; Fisseha, R.; Gascho, A.; Gysel, M.; Nyeki, S.; et al. Secondary Organic Aerosols from Anthropogenic and Biogenic Precursors. *Faraday Discuss.* **2005**, *130*, 265−278.

(8) Heaton, K. J.; Dreyfus, M. A.; Wang, S.; Johnston, M. V. Oligomers in the Early State of Biogenic Secondary Organic Aerosol. *Environ. Sci. Technol.* **2007**, *41*, 6129−6136.

(9) Virtanen, A.; Joutsensaari, J.; Koop, T.; Kannosto, J.; Yli-Pirilä, P.; Leskinen, J.; Mäkelä, J. M.; Holopainen, J. K.; Pöschl, U.; Kulmala, M.; et al. An Amorphous Solid State of Biogenic Secondary Organic Aerosol Particles. *Nature (London, U.K.)* **2010**, *467*, 824−827.

(10) Koop, T.; Bookhold, J.; Shiraiwa, M.; Pöschl, U. Glass Transition and Phase State of Organic Compounds: Dependency on Molecular Properties and Implications for Secondary Organic Aerosols in the Atmosphere. *Phys. Chem. Chem. Phys.* **2011**, *13*, 19238−19255.

(11) Renbaum-Wolff, L.; Grayson, J. W.; Bateman, A. P.; Kuwata, M.; Sellier, M.; Murray, B. J.; Shilling, J. E.; Martin, S. T.; Bertram, A. K. Viscosity of α-Pinene Secondary Organic Material and Implications for Particle Growth and Reactivity. *Proc. Natl. Acad. Sci. U.S.A.* **2013**, *110*, 8014−8019.

(12) Ensberg, J. J.; Hayes, P. L.; Jimenez, J. L.; Gilman, J. B.; Kuster, W. C.; de Gouw, J. A.; Holloway, J. S.; Seinfeld, J. H. Emission Factor Ratios, SOA Mass Yields, and the Impact of Vehicular Emissions on SOA Formation. *Atmos. Chem. Phys.* **2013**, *14*, 2383−2397.

(13) Bahreini, R.; Middlebrook, A. M.; de Gouw, J. A.; Warneke, C.; Trainer, M.; Brock, C. A.; Stark, H.; Brown, S. S.; Dube, W. P.; Gilman, J. B.; et al. Gasoline Emissions Dominate over Diesel in Formation of Secondary Organic Aerosol Mass. *Geophys. Res. Lett.* **2012**, *39*, L06805.

(14) Gentner, D. R.; Isaacman, G.; Worton, D. R.; Chan, A. W. H.; Dallmann, T. R.; Davis, L.; Liu, S.; Day, D. A.; Russell, L. M.; Wilson, K. R.; et al. Elucidating Secondary Organic Aerosol from Diesel and Gasoline Vehicles through Detailed Characterization of Organic Carbon Emissions. *Proc. Natl. Acad. Sci. U.S.A.* **2012**, *109*, 18318−18323.

(15) Zhang, H.; Ruehl, C. R.; Chan, A. W. H.; Nah, T.; Worton, D. R.; Isaacman, G.; Goldstein, A. H.; Wilson, K. R. OH-Initiated Heterogeneous Oxidation of Cholestane: A Model System for Understanding the Photochemical Aging of Cyclic Alkane Aerosols. *J. Phys. Chem. A* **2013**, *117*, 12449−12458.

(16) Reisen, F.; Aschmann, S. M.; Atkinson, R.; Arey, J. 1,4-Hydroxycarbonyl Products of the OH Radical-Initiated Reactions of C_5-C_8 *n*-Alkanes in the Presence of NO. *Environ. Sci. Technol.* **2005**, *39*, 4447−4453.

(17) Baker, J.; Arey, J.; Atkinson, R. Formation and Reaction of Hydroxycarbonyls from the Reaction of OH Radicals with 1,3-Butadiene and Isoprene. *Environ. Sci. Technol.* **2005**, *39*, 4091−4099.

(18) Schauer, J. J.; Kleeman, M. J.; Cass, G. R.; Simoneit, B. R. T. Measurement of Emissions from Air Pollution Sources. 2. C_1 through C_{30} Organic Compounds from Medium Duty Diesel Trucks. *Environ. Sci. Technol.* **1999**, *33*, 1578−1587.

(19) Schauer, J. J.; Kleeman, M. J.; Cass, G. R.; Simoneit, B. R. T. Measurement of Emissions from Air Pollution Sources. 5. C_1−C_{32}

Organic Compounds from Gasoline-Powered Motor Vehicles. *Environ. Sci. Technol.* **2002**, *36*, 1169−1180.
(20) Isaacman, G.; Wilson, K. R.; Chan, A. W. H.; Worton, D. R.; Kimmel, J. R.; Nah, T.; Hohaus, T.; Gonin, M.; Kroll, J. H.; Worsnop, D. R.; et al. Improved Resolution of Hydrocarbon Structures and Constitutional Isomers in Complex Mixtures Using Gas Chromatography-Vacuum Ultraviolet-Mass Spectrometry. *Anal. Chem.* **2012**, *84*, 2335−2342.
(21) Ruehl, C. R.; Nah, T.; Isaacman, G.; Worton, D. R.; Chan, A. W. H.; Kolesar, K. R.; Cappa, C. D.; Goldstein, A. H.; Wilson, K. R. The Influence of Molecular Structure and Aerosol Phase on the Heterogeneous Oxidation of Normal and Branched Alkanes by OH. *J. Phys. Chem. A* **2013**, *117*, 3990−4000.
(22) Lim, Y. B.; Ziemann, P. J. Chemistry of Secondary Organic Aerosol Formation from OH Radical-Initiated Reactions of Linear, Branched, and Cyclic Alkanes in the Presence of NO_x. *Aerosol Sci. Technol.* **2009**, *43*, 604−619.
(23) Lim, Y. B.; Ziemann, P. J. Effects of Molecular Structure on Aerosol Yields from OH Radical-Initiated Reactions of Linear, Branched, and Cyclic Alkanes in the Presence of NO_x. *Environ. Sci. Technol.* **2009**, *43*, 2328−2334.
(24) Lim, Y. B.; Ziemann, P. J. Products and Mechanism of Secondary Organic Aerosol Formation from Reactions of *n*-Alkanes with OH Radicals in the Presence of NO_x. *Environ. Sci. Technol.* **2005**, *39*, 9229−9236.
(25) Ziemann, P. J. Formation of Alkoxyhydroperoxy Aldehydes and Cyclic Peroxyhemiacetals from Reactions of Cyclic Alkenes with Ozone in the Presence of Alcohols. *J. Phys. Chem. A* **2003**, *107*, 2048−2060.
(26) Tkacik, D. S.; Presto, A. A.; Donahue, N. M.; Robinson, A. L. Secondary Organic Aerosol Formation from Intermediate-Volatility Organic Compounds: Cyclic, Linear, and Branched Alkanes. *Environ. Sci. Technol.* **2012**, *46*, 8773−8781.
(27) Presto, A. A.; Miracolo, M. A.; Donahue, N. M.; Robinson, A. L. Secondary Organic Aerosol Formation from High-NO_x Photo-Oxidation of Low Volatility Precursors: *n*-Alkanes. *Environ. Sci. Technol.* **2010**, *44*, 2029−2034.
(28) Yee, L. D.; Craven, J. S.; Loza, C. L.; Schilling, K. A.; Ng, N. L.; Canagaratna, M. R.; Ziemann, P. J.; Flagan, R. C.; Seinfeld, J. H. Secondary Organic Aerosol Formation from Low-NO_x Photooxidation of Dodecane: Evolution of Multigeneration Gas-Phase Chemistry and Aerosol Composition. *J. Phys. Chem. A* **2012**, *116*, 6211−6230.
(29) Yee, L. D.; Craven, J. S.; Loza, C. L.; Schilling, K. A.; Ng, N. L.; Canagaratna, M. R.; Ziemann, P. J.; Flagan, R. C.; Seinfeld, J. H. Effect of Chemical Structure on Secondary Organic Aerosol Formation from C_{12} Alkanes. *Atmos. Chem. Phys.* **2013**, *13*, 11121−11140.
(30) Craven, J. S.; Yee, L. D.; Ng, N. L.; Canagaratna, M. R.; Loza, C. L.; Schilling, K. A.; Yatavelli, R. L. N.; Thornton, J. A.; Ziemann, P. J.; Flagan, R. C.; et al. Analysis of Secondary Organic Aerosol Formation and Aging Using Positive Matrix Factorization of High-Resolution Aerosol Mass Spectra: Application to the Dodecane Low-NO_x System. *Atmos. Chem. Phys.* **2012**, *12*, 11795−11817.
(31) Craven, J. S.; Yee, L. D.; Ng, N. L.; Canagaratna, M. R.; Loza, C. L.; Schilling, K. A.; Yatavelli, R. L. N.; Thornton, J. A.; Ziemann, P. J.; Flagan, R. C.; Seinfeld, J. H. Analysis of Secondary Organic Aerosol Formation and Aging Using Positive Matrix Factorization of High-Resolution Aerosol Mass Spectra: Application to the Dodecane Low-NO_x System. *Atmos. Chem. Phys.* **2012**, *12*, 11795−11817.
(32) Yee, L. D.; Craven, J. S.; Loza, C. L.; Schilling, K. A.; Ng, N. L.; Canagaratna, M. R.; Ziemann, P. J.; Flagan, R. C.; Seinfeld, J. H. Effect of Chemical Structure on Secondary Organic Aerosol Formation from C_{12} Alkanes. *Atmos. Chem. Phys.* **2013**, *13*, 11121−11140.
(33) Lambe, A. T.; Onasch, T. B.; Croasdale, D. R.; Wright, J. P.; Martin, A. T.; Franklin, J. P.; Massoli, P.; Kroll, J. H.; Canagaratna, M. R.; Brune, W. H.; et al. Transitions from Functionalization to Fragmentation Reactions of Laboratory Secondary Organic Aerosol Generated from the OH Oxidation of Alkane Precursors. *Environ. Sci. Technol.* **2012**, *46*, 5430−5437.
(34) Tkacik, D. S.; Presto, A. A.; Donahue, N. M.; Robinson, A. L. Secondary Organic Aerosol Formation from Intermediate-Volatility Organic Compounds: Cyclic, Linear and Branched Alkanes. *Environ. Sci. Technol.* **2012**, *46*, 8773−8781.
(35) Zhang, X.; Schwantes, R. H.; Coggon, M. M.; Loza, C. L.; Schilling, K. A.; Flagan, R. C.; Seinfeld, J. H. Role of Ozone in SOA Formation from Alkane Photooxidation. *Atmos. Chem. Phys.* **2013**, *14*, 1733−1753.
(36) Shiraiwa, M.; Yee, L. D.; Schilling, K. A.; Loza, C. L.; Craven, J. S.; Zuend, A.; Ziemann, P. J.; Seinfeld, J. H. Size Distribution Dynamics Reveal Particle-Phase Chemistry in Organic Aerosol Formation. *Proc. Natl. Acad. Sci. U.S.A.* **2013**, *110*, 11746−11750.
(37) Lim, Y. B.; Ziemann, P. J. Kinetics of the Heterogeneous Conversion of 1,4-Hydroxycarbonyls to Cyclic Hemiacetals and Dihydrofurans on Organic Aerosol Particles. *Phys. Chem. Chem. Phys.* **2009**, *11*, 8029.
(38) De Haan, D. O.; Tolbert, M. A.; Jimenez, J. L. Atmospheric Condensed-Phase Reactions of Glyoxal with Methylamine. *Geophys. Res. Lett.* **2009**, *36*, L11819.
(39) Lim, Y. B.; Ziemann, P. J. Chemistry of Secondary Organic Aerosol Formation from OH Radical-Initiated Reactions of Linear, Branched, and Cyclic Alkanes in the Presence of NO_x. *Aerosol Sci. Technol.* **2009**, *43*, 604−619.
(40) De Haan, D. O.; Corrigan, A. L.; Smith, K. W.; Stroik, D. R.; Turley, J. J.; Lee, F. E.; Tolbert, M. A.; Jimenez, J. L.; Cordova, K. E.; Ferrell, G. R. Secondary Organic Aerosol-Forming Reactions of Glyoxal with Amino Acids. *Environ. Sci. Technol.* **2009**, *43*, 2818−2824.
(41) Nguyen, T. B.; Laskin, A.; Laskin, J.; Nizkorodov, S. A. Brown Carbon Formation from Ketoaldehydes of Biogenic Monoterpenes. *Faraday Discuss.* **2013**, *165*, 473−494.
(42) Loza, C. L.; Craven, J. S.; Yee, L. D.; Coggon, M. M.; Schwantes, R. H.; Shiraiwa, M.; Zhang, X.; Schilling, K. A.; Ng, N. L.; Canagaratna, M. R.; et al. Secondary Organic Aerosol Yields of 12-Carbon Alkanes. *Atmos. Chem. Phys.* **2014**, *14*, 1423−1439.
(43) Compernolle, S.; Ceulemans, K.; Müller, J. F. EVAPORATION: A New Vapour Pressure Estimation Method for Organic Molecules Including Non-Additivity and Intramolecular Interactions. *Atmos. Chem. Phys.* **2011**, *11*, 9431−9450.
(44) Jenkin, M. E.; Saunders, S. M.; Pilling, M. J. The Tropospheric Degradation of Volatile Organic Compounds: A Protocol for Mechanism Development. *Atmos. Environ.* **1997**, *31*, 81−104.
(45) Cody, R. B.; Laramee, J. A.; Durst, H. D. Versatile New Ion Source for the Analysis of Materials in Open Air under Ambient Conditions. *Anal. Chem.* **2005**, *77*, 2297−2302.
(46) Cody, R. B. Observation of Molecular Ions and Analysis of Nonpolar Compounds with the Direct Analysis in Real Time Ion Source. *Anal. Chem.* **2009**, *81*, 1101−1107.
(47) Shelley, J. T.; Wiley, J. S.; Chan, G. C. Y.; Schilling, G. D.; Ray, S. J.; Hieftje, G. M. Characterization of Direct-Current Atmospheric Pressure Discharges Useful for Ambient Desorption/Ionization Mass Spectrometry. *J. Am. Soc. Mass Spectrom.* **2009**, *20*, 837−844.
(48) Harris, G. A.; Fernandez, F. M. Simulations and Experimental Investigation of Atmospheric Transport in an Ambient Metastable-Induced Chemical Ionization Source. *Anal. Chem.* **2009**, *81*, 322−329.
(49) Nilles, J. M.; Connell, T. R.; Durst, H. D. Quantitation of Chemical Warfare Agents Using the Direct Analysis in Real Time (DART) Technique. *Anal. Chem.* **2009**, *81*, 6744−6749.
(50) Goldstein, A. H.; Galbally, I. E. Known and Unknown Organic Constituents in the Earth's Atmosphere. *Environ. Sci. Technol.* **2007**, *41*, 1514−1521.
(51) Taylor, J.; Hall, C. R. L.; Thomas, H. The Thermochemistry of Propellant Explosives. *J. Phys. Colloid Chem.* **1947**, *51*, 580−592.
(52) Self, R. L.; Wu, W.-H. Rapid Qualitative Analysis of Phthalates Added to Food and Nutraceutical Products by Direct Analysis in Real Time/Orbitrap Mass Spectrometry. *Food Control* **2012**, *25*, 13−16.
(53) Rothenbacher, T.; Schwack, W. Rapid Identification of Additives in Poly(vinyl chloride) Lid Gaskets by Direct Analysis in Real Time Ionisation and Single-Quadrupole Mass Spectrometry. *Rapid Commun. Mass Spectrom.* **2010**, *24*, 21−29.

(54) Lias, S. G.; Bartmess, J. E. *Proton Affinity and Gas Phase Basicity*. http://webbook.nist.gov/chemistry/ion/#GB (accessed 01/27/2014).
(55) Hunter, E. P. L.; Lias, S. G. Evaluated Gas Phase Basicities and Proton Affinities of Molecules: An Update. *J. Phys. Chem. Ref. Data* **1998**, *27*, 413−656.
(56) Van Krevelen, D. W. Graphical-Statistical Method for the Study of Structure and Reaction Processes of Coal. *Fuel* **1950**, *24*, 269−284.
(57) Kim, S.; Kramer, R. W.; Hatcher, P. G. Graphical Method for Analysis of Ultrahigh-Resolution Broadband Mass Spectra of Natural Organic Matter: The Van Krevelen Diagram. *Anal. Chem.* **2003**, *75*, 5336−5344.
(58) Wu, Z.; Rodgers, R. P.; Marshall, A. G. Two- and Three-Dimensional Van Krevelen Diagrams: A Graphical Analysis Complementary to the Kendrick Mass Plot for Sorting Elemental Compositions of Complex Organic Mixtures Based on Ultrahigh-Resolution Broadband Fourier Transform Ion Cyclotron Resonance Mass Measurements. *Anal. Chem.* **2004**, *76*, 2511−2516.
(59) Heald, C. L.; Kroll, J. H.; Jimenez, J. L.; Docherty, K. S.; DeCarlo, P. F.; Aiken, A. C.; Chen, Q.; Martin, S. T.; Farmer, D. K.; Artaxo, P. A Simplified Description of the Evolution of Organic Aerosol Composition in the Atmosphere. *Geophys. Res. Lett.* **2010**, *37*, L08803.
(60) Ng, N. L.; Canagaratna, M. R.; Jimenez, J. L.; Chhabra, P. S.; Seinfeld, J. H.; Worsnop, D. R. Changes in Organic Aerosol Composition with Aging Inferred from Aerosol Mass Spectra. *Atmos. Chem. Phys.* **2011**, *11*, 6465−6474.
(61) Chhabra, P. S.; Ng, N. L.; Canagaratna, M. R.; Corrigan, A. L.; Russell, L. M.; Worsnop, D. R.; Flagan, R. C.; Seinfeld, J. H. Elemental Composition and Oxidation of Chamber Organic Aerosol. *Atmos. Chem. Phys.* **2011**, *11*, 8827−8845.
(62) Lambe, A. T.; Onasch, T. B.; Massoli, P.; Croasdale, D. R.; Wright, J. P.; Ahern, A. T.; Williams, L. R.; Worsnop, D. R.; Brune, W. H.; Davidovits, P. Laboratory Studies of the Chemical Composition and Cloud Condensation Nuclei Activity of Secondary Organic Aerosol and Oxidized Primary Organic Aerosol. *Atmos. Chem. Phys.* **2011**, *11*, 8913−8928.
(63) Hall, W. A., IV; Johnston, M. V. Oligomer Formation Pathways in Secondary Organic Aerosol from MS and MS/MS Measurements with High Mass Accuracy and Resolving Power. *J. Am. Soc. Mass Spectrom.* **2012**, *23*, 1097−1108.
(64) Dibble, T. S. Cyclization of 1,4-Hydroxycarbonyls Is Not a Homogeneous Gas-Phase Process. *Chem. Phys. Lett.* **2007**, *447*, 5−9.
(65) Atkinson, R.; Arey, J.; Aschmann, S. M. Atmospheric Chemistry of Alkanes: Review and Recent Developments. *Atmos. Environ.* **2008**, *42*, 5859−5871.
(66) De Haan, D. O.; Corrigan, A. L.; Smith, K. W.; Stroik, D. R.; Turley, J. J.; Lee, F. E.; Tolbert, M. A.; Jimenez, J. L.; Cordova, K. E.; Ferrell, G. R. Secondary Organic Aerosol-Forming Reactions of Glyoxal with Amino Acids. *Environ. Sci. Technol.* **2009**, *43*, 2818−2824.
(67) Ziemann, P. J. Aerosol Products, Mechanisms, and Kinetics of Heterogeneous Reactions of Ozone with Oleic Acid in Pure and Mixed Particles. *Faraday Discuss.* **2005**, *130*, 469−490.
(68) Markert, M.; Mulzer, M.; Schetter, B.; Mahrwald, R. Amine-Catalyzed Direct Aldol Addition. *J. Am. Chem. Soc.* **2007**, *129*, 7258−7259.
(69) Liu, S.; Day, D. A.; Shields, J. E.; Russell, L. M. Ozone-Driven Daytime Formation of Secondary Organic Aerosol Containing Carboxylic Acid Groups and Alkane Groups. *Atmos. Chem. Phys.* **2011**, *11*, 8321−8341.
(70) Lim, Y. B.; Ziemann, P. J. Kinetics of the Heterogeneous Conversion of 1,4-Hydroxycarbonyls to Cyclic Hemiacetals and Dihydrofurans on Organic Aerosol Particles. *Phys. Chem. Chem. Phys.* **2009**, *11*, 8029−8039.